Summer 2021

Mantle flow systems associated with slab subduction and absolute plate motion in Alaska constrained by shear wave splitting analyses

Yuchen Yang

Department: Geosciences and Geological and Petroleum Engineering

MANTLE FLOW SYSTEMS ASSOCIATED WITH SLAB SUBDUCTION AND ABSOLUTE PLATE MOTION IN ALASKA CONSTRAINED BY SHEAR WAVE SPLITTING ANALYSES

by

YUCHEN YANG

A DISSERTATION

Presented to the Graduate Faculty of the

MISSOURI UNIVERSITY OF SCIENCE AND TECHNOLOGY

In Partial Fulfillment of the Requirements for the Degree

DOCTOR OF PHILOSOPHY

in

GEOLOGY AND GEOPHYSICS

2021

Approved by:

Stephen Gao, Advisor
Kelly Liu, Co-Advisor
David Wronkiewicz
Ryan Smith
Baojun Bai
Xiaofei Fu

PUBLICATION DISSERTATION OPTION

This dissertation consists of the following two articles, which will be submitted for publications as follows:

Paper I, found on pages 3-42, is intended for submission to *the journal of Geochemistry, Geophysics, Geosystems.*

Paper II, found on pages 43-70, is intended for submission to *the journal of Geophysical Research: Solid Earth.*

ABSTRACT

Alaska has long been recognized as a geologically complex region with a sharp contrast in tectonic activity between southern and northern Alaska. While the former is characterized by the subduction of the geometrically varying Pacific-Yakutat plate beneath the North American plate, the latter has a mostly stable cratonic setting. To investigate the mantle flow fields beneath Alaska and understand the influence of the subduction process on regional mantle dynamics, a total of 2790 pairs of well-defined teleseismic shear wave splitting (SWS) measurements recorded from 379 stations are obtained and analyzed. In addition, 247 pairs of SWS results from local earthquake events are measured to isolate contribution of the mantle wedge to the teleseismic shear wave splitting. We obtain well-defined two-layered anisotropy models in three areas in southern Alaska. The observations revealed several mantle flow fields, including trench-parallel flow beneath the Pacific slab, trench-normal flow beneath the flat Yakutat slab, toroidal flow around the Pacific-Yakutat slab edge, absolute plate motion-parallel flow in the stable cratonic area, and deflected flow around the deep continental keel in northern and possibly western Alaska. The presence of a slab edge and conflicting conclusions from previous shear wave splitting studies motivated us for an in-depth analysis of the splitting measurements in southcentral Alaska. The results indicate that the sub-slab flow, which is driven by slab roll-back, may separate into two branches at the edge: One flows anticlockwise to the wedge, and the other continues flowing to the east of the study area.

ACKNOWLEDGMENTS

First, I would like to express my sincere appreciation to my advisor Dr. Stephen Gao and my co-advisor Dr. Kelly Liu for their valuable academic guidance and day-to-day attention during the past several years. I feel truly blessed to pursue and accomplish my PhD degree under their suggestions and encouragements. Their diligence and tenacity on research will always inspire me to be a hardworking person.

Besides my advisors, I want to convey my gratitude to the rest of my dissertation committee members, Dr. David Wronkiewicz, Dr. Ryan Smith, Dr. Baojun Bai, and Dr. Xiaofei Fu for their constructive suggestions and comments. I also want to thank my colleagues and group members for academic discussions and teamwork. Furthermore, I want to express my thanks to the staffs in Geosciences and Geological and Petroleum Engineering department, Sharon Lauck and Patty Robertson, for their plentiful assistance, and to my graduate advisor Kathy Wagner and my international advisor Shawna Holle for the instructions on a list of required forms.

Last but not least, I would like to show my heartfelt gratefulness to my parents and family members for their continuous support and sacrifices. Without their encouragements and spurs, I cannot accomplish my research work and dissertation smoothly.

TABLE OF CONTENTS

SECTION

LIST OF ILLUSTRATIONS

PAPER I Page

PAPER II

NOMENCLATURE

Symbol	Description
ϕ	Fast Orientation
δt	Splitting Time

SECTION

1. INTRODUCTION

As demonstrated by numerous previous investigations, shear wave splitting (SWS) analysis using P-to-S converted phases (PKS, SKS, SKKS which are collectively termed as "XKS" hereafter) at the core-mantle boundary, has been extensively utilized to delineate spatial distributions of seismic azimuthal anisotropy and probe corresponding mantle dynamics (Long & Silver, 2009; Savage, 1999; Silver & Chan, 1991). The Transportable Array (TA) component of the USArray project, which started in 2011 and has recently completed its coverage of the contiguous Alaska region, has produced a broadband seismic data set at stations that are ~85km apart from each other with unprecedented quality and spatial coverage, permitting the deep study of the earth's interior beneath the Alaska region.

The dissertation is mainly composed of two parts. The first part proposes the multiple mantle flow fields and related anisotropic structures beneath the entire Alaska region, based on the splitting measurements. Even though the mantle flow system in Alaska has been investigated by many previous SWS studies (e.g. Christensen & Abers, 2010; Hanna & Long, 2012; McPherson et al., 2020; Perttu et al., 2014; Venereau et al., 2019), most of the studies lack a broad station coverage and sufficient seismic data. By contrast, this study utilizes data with a recording period of ~30 years from late 1988 to March 2019. Moreover, the data are obtained by stations that cover the entire Alaska region. Such unprecedented data amount from three seismic phases significantly

improved the azimuthal coverage, enabling us to characterize complex anisotropy structures and subsequently obtaining a more reliable three-dimensional mantle flow model.

The second part is an in-depth investigation of the mantle dynamics in the eastern Alaska subduction zone (EASZ) where complicated splitting patterns are observed. The tectonic setting here is the most complicated throughout the entire Alaska region for the varying slab geometry and a sharp slab edge. However, detailed studies in this particular region are rare. In this study, 971 pairs of XKS and 65 pairs of local S splitting measurements are obtained. We visually examine all the XKS results to identify simple and complex anisotropy. Finally, we construct a new three-dimensional mantle flow model based on the observed anisotropy.

PAPER

I. MANTLE FLOW SYSTEMS ASSOCIATED WITH SLAB SUBDUCTION AND ABSOLUTE PLATE MOTION IN ALASKA CONSTRAINED BY SHEAR WAVE SPLITTING ANALYSES

ABSTRACT

The Aleutian-Alaska subduction zone is one of the most geologically complex regions in the world for its varying slab geometry, uncommon subducting type, and atypical volcanic activities. The sharp contrast between the subduction-impacted southern Alaska and the tectonically quiescent northern area makes Alaska an optimal locale for investigating the linkage between surface geological features and dynamic processes in the Earth's deep interior. In this study, we obtain 2790 pairs of teleseismic shear wave splitting measurements from three seismic phases (PKS, SKS, SKKS which are collectively termed as "XKS" hereafter) recorded by 379 USArray and other stations to provide additional constraints on mantle flow and deformation models. Using all the three XKS phases and combining results from nearby stations significantly improved the azimuthal coverage, and consequently led to better constrained two-layered models of anisotropy in three areas in southern Alaska than those obtained by previous studies. In addition, 247 pairs of local S splitting results are measured to isolate contribution of the mantle wedge to the observed XKS splitting. The observations suggest the existence of different flow systems in the upper mantle beneath the Alaska region, including trench-parallel flow beneath the normal-dipping Pacific slab in the Aleutian arcs, trench-normal flow beneath the flat subduction region, toroidal flow around a sharp slab edge, absolute

plate motion-parallel flow in the stable cratonic area, and deflected flow around the deep continental keel in northern and possibly western Alaska.

1. INTRODUCTION

The Pacific plate has been subducting beneath the North American Plate northwestward along the Aleutian trench since mid-Jurassic (Fisher & Magoon, 1978). At the present time, the oblique convergence along the Alaska portion of the trench has a rate of approximately 50 mm/yr (Figure 1) (DeMets et al., 2010; Fisher & Magoon, 1978; Wang & Tape, 2014). The subduction process has produced substantial seismicity and volcanic activity, and intensive continental deformation along the convergent plate margin (Finzel et al., 2011; Hanna & Long, 2012; Venereau et al., 2019). In contrast, the tectonically quiescent area north of the Brooks Range is underlain by a cold lithospheric root (Jiang et al., 2018). Whether the subduction-related mantle flow system has reached this area is not clear and is one of the objectives of the current study.

1.1. GEOLOGICAL SETTING OF THE ALEUTIAN-ALASKA SUBDUCTION ZONE

The subduction of the Pacific Plate beneath the North American Plate along the Aleutian trench (Figure 1) is characterized by a n○ormal dip angle of ~40° (measured from the horizontal), while in southcentral Alaska the active tectonic setting is dominated by the flat subduction of the Yakutat terrane which is marked by a shallower than normal Wadati-Benioff zone with a dip angle smaller than 5° (Bauer et al., 2014; Christensen & Abers, 2010). The Yakutat terrane is believed to have originated as an oceanic plateau

and subsequently migrated northward along the dextral strike-slip fault, named Queen Charlotte/Fairweather (QC-F) Fault (Figure 1) (Bauer et al., 2014; Christeson et al., 2010; Eberhart-Phillips et al., 2006). The Yakutat terrane consists of the northwestward shallow-dip Yakutat slab as well as the southeastern unsubducted terrane (Finzel et al., 2011; Plafker & Berg, 1994), the latter of which has collided into the southeast corner of Alaska, forming the region referred to as the Yakutat Collision Zone (McPherson et al., 2020) (Figure 1). The complicated subducting system in southern Alaska has led to some atypical magmatic features. The most enigmatic one is the Wrangell Volcanic Field (WVF). Preece & Hart (1994) interpret the WVF as being composed of three different geochemical trends, suggesting different magma sources and complicated melting processes. Finzel and Trop (2011) indicate that the northwestward Yakutat subduction may account for the northwestward volcanism progression in the WVF (Richter et al., 1990).

1.2. UPPER MANTLE STRUCTURE

To reveal the subsurface structures and probe the relationship between the large-scale geological features with the deformations associated with the subduction, numerous seismic tomography studies have been conducted in southern Alaska (e.g. Gou et al., 2019; Jiang et al., 2018; Martin-Short et al., 2018; Qi et al., 2007; Zhao et al., 1995). The Pacific slab is imaged as a strip of high-velocity anomalies that steeply sinks toward the northwest and reaches its maximum depth of ~450-500 km (Gou et al., 2019), while the high-velocity feature representing the shallower Yakutat slab only appears within the top ~100 km (Martin-Short et al., 2018).

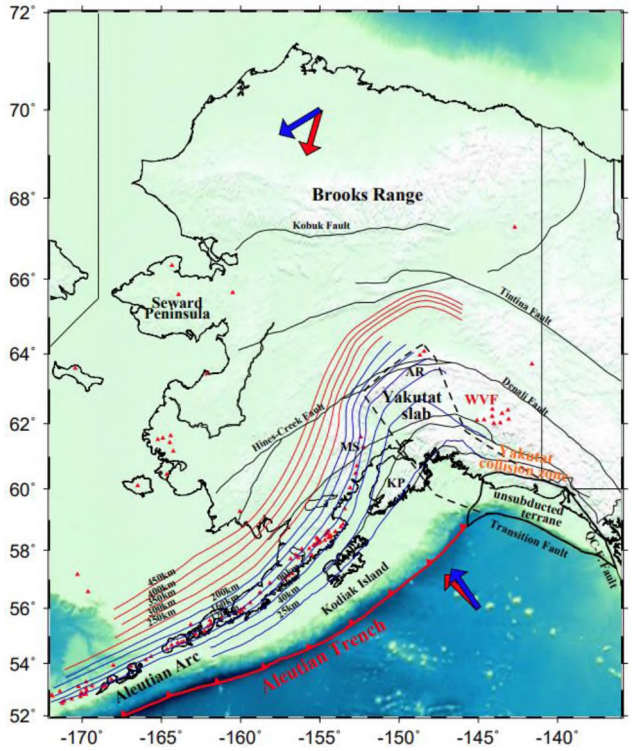

Figure 1. A topographic relief map of the Alaska region showing major tectonic features. The Yakutat Terrane is delineated by black line (Eberhart-Phillips et al., 2006). Red triangles indicate active volcanoes. Contour lines of the depth of the Pacific-Yakutat slab are shown in blue (200 km or shallower) and red lines (deeper than 200 km) (Gou et al., 2019). Blue and red arrows represent the absolute plate motion direction based on the NNR-MORVEL56 model (Argus et al., 2011) and the HS3-NUVEL-1A model (Gripp & Gordon, 2002), respectively. KP: Kenai Peninsula. AR: Alaska Range. QC-F. Fault: Queen Charlotte/Fairweather Fault System.

Additionally, a high-velocity structure is imaged and interpreted as a possible Wrangell slab (Gou et al., 2019; Jiang et al., 2018; Yang & Gao, 2020), while Martin-Short et al. (2018) observe a sharp termination of S-wave anomaly beneath the WVF, indicating the absence of the Wrangell slab. Gou et al. (2019) also find a slab gap structure between the Wrangell slab and a possible aseismic slab portion to the northwest. Such a structure may serve as a channel in transporting hot mantle materials and explains the existence of adakitic magma in the WVF (Preece & Hart, 2004). Considerable

differences in the various seismic tomography studies in Alaska have led to conflicting conclusions on the formation mechanisms of the WVF and thus understanding the mantle dynamics may provide additional constraints on the geodynamic models, as demonstrated below.

1.3. SHEAR WAVE SPLITTING AND SEISMIC ANISOTROPY

Shear wave splitting analysis is the most frequently used technique for characterizing mantle dynamics and providing critical constraints on mantle flow models (Silver & Chan, 1991). When a P-to-S converted wave from the core-mantle boundary (SKS, SKKS, and PKS, hereafter collectively called XKS) propagates through an azimuthally anisotropic layer, the shear wave would split into two components with orthogonally polarized directions and different traveling speed (Long & Silver, 2009; Savage, 1999; Silver, 1996). Two splitting parameters, the polarization orientation of the fast component (or fast orientation) and the arrival time difference between the fast and slow components (or splitting time), are measured to quantify the orientation and strength of seismic anisotropy, respectively.

Under normal upper mantle temperature and pressure conditions, seismic azimuthal anisotropy is mainly caused by the lattice preferred orientation (LPO) of the crystallographic axes of anisotropic minerals such as olivine, as indicated by laboratory experiments and geodynamic modeling studies (Zhang & Karato, 1995). In the asthenosphere, flow-parallel LPO is most commonly observed and is considered to be generated by simple shear associated with various tectonic processes, such as the absolute plate motion (APM), slab subduction and rollback (Long & Becker, 2010; Schellart,

2004). Laboratory and observational studies suggest that the fast orientations of the XKS splitting are dominantly flow-parallel (Silver & Chan, 1988; Vauchez & Nicolas, 1991) except for areas dominated by high stress, low temperatures and moderate water capacity such as the area near the tip of the mantle wedge (Karato et al., 2008), where a "B-type" fabric produces flow-perpendicular fast orientations. Furthermore, in the lithosphere, horizontal compression may lead to LPO normal to the maximum horizontal shortening direction (e.g. Chastel et al., 1993; Francis, 1969; Hess, 1964; Silver, 1996; Silver & Chan, 1991), and oriented vertical lithospheric scale dikes may produce azimuthal anisotropy with a fast orientation parallel to the dikes (Gao et al., 1997).

Most of the XKS investigations are conducted under the assumption of simple anisotropy that refers to anisotropy from a single anisotropic layer with a horizontal axis of symmetry. This ideal condition produces similar splitting parameters with respect to the arriving azimuth of the events (back-azimuth or BAZ). In areas dominated by simple anisotropy, station-averaged splitting parameters can objectively reflect the anisotropy characteristics. Departures from the ideal conditions of simple anisotropy are termed as complex anisotropy (Silver & Savage, 1994), and the most common form of complex anisotropy structure consists of two anisotropic layers, each with a horizontal axis of symmetry. This form of complex anisotropy is characterized by systematic azimuthal variations of the individual splitting parameters with a 90^{o} periodicity. If a station is located near the boundary between two or more areas with different anisotropic characteristics, the observed anisotropy at the station may also vary azimuthally (referred to as spatially varying anisotropy hereinafter), although the variation may not necessarily possess a 90^{o} periodicity (Liu & Gao, 2013).

XKS splitting measurements in a subduction zone setting reflect the combined effect from anisotropy in the mantle wedge, subducting slab, sub-slab mantle, as well as the overriding plate (Long & Wirth, 2013). Slab rollback has been proposed to be responsible for the trench-perpendicular 2-D corner flow in the mantle wedge and the trench-parallel flow in the sub-slab region (e.g. Fouch & Fischer, 1996; Hall et al., 2000; Russo & Silver, 1994). Furthermore, sub-slab entrained flow caused by the coupling between the subducting slab and sub-slab mantle can also induce trench-perpendicular azimuthal anisotropy (Russo & Silver, 1994). Near the edge of a subducting slab, sub-slab mantle materials may flow around the slab edge driven by slab rollback (e.g. Becker & Faccenna, 2009; Long & Wirth, 2013; Russo & Silver, 1994). In the wedge, such flow may either join the trench-perpendicular 2-D corner flow (e.g. Long & Silver, 2008, 2009; Russo & Silver, 1994; Schellart, 2004; Stegman et al., 2006) or become trench-parallel due to the low viscosity and high flux speed (Jadamec & Billen, 2010, 2012).

2. PREVIOUS SWS STUDIES AND RATIONALE OF THE PRESENT STUDY

A number of SWS studies have been conducted in Alaska and adjacent areas over the past decades (Figure 2). Using data from a few seismic stations in the vicinity of the Denali fault, several SWS studies (Figure 2) propose that fault-parallel fast orientations in the shear zones are associated with the transpressional deformation ascribed to the combination of parallel strike-slip motion of the Denali fault and the orogenic activities (Rasendra et al., 2014; Silver & Chan, 1991; Vinnik et al., 1992). Based on splitting parameters from local earthquakes in the Shumagin islands of the Aleutian Arc, arc-

parallel fast orientations and an increase in splitting times with the focal depth are found, suggesting that the observed anisotropy is sourced from the mantle wedge (Yang et al., 1995).

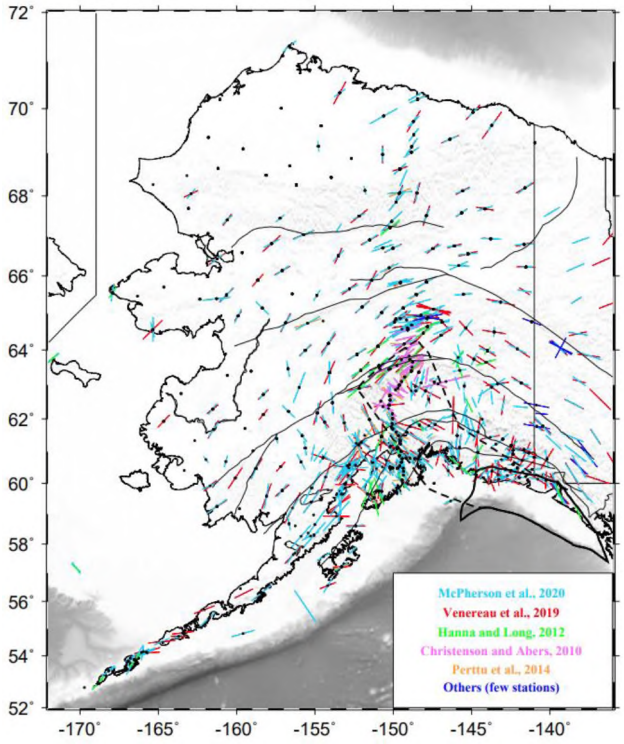

Figure 2. Previous shear wave splitting measurements. Bars with different colors represent measurements from different studies, while black dots indicate stations used in this study. Note that the dark blue bars are measurements from several studies using few stations (Rasendra et al., 2014; Silver & Chan, 1991; Vinnik et al., 1992; Yang et al., 1995).

With the recent development of portable seismic networks in the Alaska region, including the USArray Transportable Array (TA), Broadband Experiment Across the Alaska Range (BEAAR), Alaska Receiving Cross Transect of the Inner Core (ARCTIC), and Multidisciplinary Observations Of Subduction (MOOS), the last decade witnessed a dramatic increase in the number of SWS measurements and improvement in the spatial

coverage by the measurements in Alaska (Figure 2). The most prominent feature from these portable stations is an ~90° change of the fast orientation near the ~70 km slab depth contour line, which separates the northern area with mostly trench-parallel and the southern area dominated by trench-normal fast orientations (Christensen & Abers, 2010; Hanna & Long, 2012; Perttu et al., 2014). Specifically, Christensen & Abers (2010) find a positive correlation between the length of the wave paths within the mantle wedge and the splitting times, implying a mantle wedge source of anisotropy. Based on the splitting measurements from 239 TA and other stations, Venereau et al. (2019) propose multiple mantle flow regimes in the entire Alaska region, including the entrained flow beneath the Yakutat slab, trench-parallel flow along the Pacific slab, toroidal flow around the slab edge, and APM-parallel flow in northern Alaska. Using the data recorded over the period of 2010-2017, McPherson et al. (2020) obtain SWS measurements at 384 TA and other stations and divide the Alaska region into six sub-regions according to different splitting patterns. They speculate the existence of complex anisotropy in the tectonic transition zones between the sub-regions, although no attempt was made to characterize the anisotropic structure using the observed azimuthal dependence of the splitting parameters.

The current study is motivated by the following factors. The most significant one is the dramatic increase in the station and azimuthal coverages as a result of the deployment of the USArray Transportable Array (TA) stations. The most recent SWS study covering Alaska (McPherson et al., 2020) used data recorded from 2010-2017, when most of the TA stations had only operated several months. In comparison, this study uses all the available data recorded prior to early 2019. As demonstrated below, the

additional data recorded between 2017 and 2019 substantially improved the station and azimuthal coverages in Alaska, and consequently improved the possibility to probe and analyze complex anisotropy quantitatively. Furthermore, the utilization of local events which characterizes seismic anisotropy in the mantle wedge may provide more constraints in investigating the regional mantle flow mechanisms. In this study, we use over-30-year seismic data obtained from both teleseismic and local earthquake events with unprecedented station and azimuthal coverages in the Alaska region, to delineate spatial distributions of seismic azimuthal anisotropy, identify and characterize the complex anisotropic structures, and propose a 3-D geodynamic model invoking different mantle flow systems to interpret the SWS observations.

3. DATA AND METHODS

The XKS and local S data used in this study were recorded by 379 broadband seismic stations (i.e. black dots in Figure 2) located in the area of 52-72° N and 172-137°W covering a recording period of 30 years from late 1988 to October 2019. The seismic data were requested from the Incorporated Research Institutions for Seismology (IRIS) Data Management Center (DMC).

The splitting parameters were measured and ranked following the procedures described in Liu & Gao (2013) and are briefly summarized below. The procedures were developed based on the minimization of transverse energy technique (Silver & Chan, 1991). Only events with a magnitude of 5.6 or greater were used for data requested from

the DMC, and the cutoff magnitude was reduced to 5.5 for events with focal depths larger than 100 km, and for local S wave splitting analysis, the cutoff magnitude is 4.0.

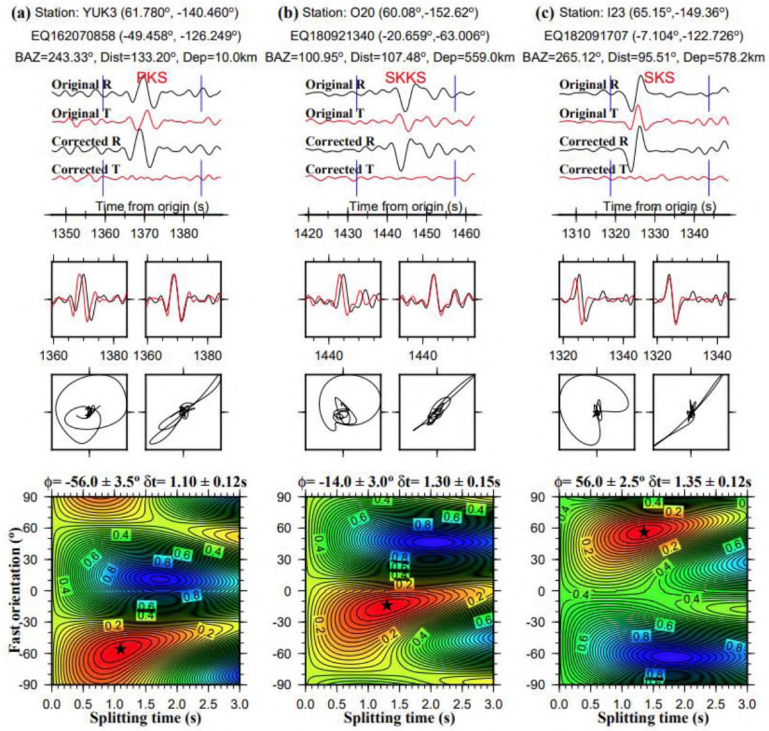

Figure 3. Examples of PKS, SKKS, and SKS splitting measurements. Each figure shows the (top) original and corrected radial and transverse components, (middle) fast and slow components before and after correction, and particle motion patterns prior to and after forwarding the slow component by the optimal splitting time, and (bottom) misfit function maps calculated by measuring the energy on the corrected transverse component. The optimal splitting parameters marked by the black stars correspond to the minimum value on the misfit function map.

Furthermore, only local events in the S-wave window (which is approximately within an angle of incidence of 35o) are used. The seismograms were initially windowed in the time period 5 s before and 20 s after the predicted time of the XKS arrival, and then were band-pass filtered in the frequency range of 0.04-0.5 Hz. The corresponding parameters for local S splitting are 5 s before and 10 s after, and 0.1-1.0 Hz. After all the

splitting parameters were automatically calculated and ranked (Liu & Gao, 2013), we manually checked all the measurements to verify and adjust the beginning and end of the XKS and local S time window, quality ranking, and band-pass filtering frequencies. The final SWS measurements were grouped into Quality A (outstanding), B (good), and C (not used), and only A and B measurements were used in the study. We also identified null measurements, which are characterized by strong XKS energy on the radial components but an absence of XKS energy on the transverse component (Silver & Chan, 1991). For a raypath that travels through an azimuthally anisotropic area (integrated over the raypath from the core-mantle boundary to the station), null measurements are only observed when the BAZ is parallel or orthogonal to the fast orientation (assuming simple anisotropy). Because well-defined splitting parameters were obtained at all the stations with one or more events having strong XKS arrivals on the radial component, null measurements are not discussed in the following. Figure 3 exhibits examples of quality A measurements of three different XKS phases recorded at different stations.

4. RESULTS

A total of 2790 pairs of well-defined (Quality A or B) XKS measurements, including 54 PKS, 91 SKKS, and 2645 SKS measurements, are obtained at 379 stations, while 247 pairs of shear wave measurements from local earthquakes are measured at 70 stations. For the XKS results, the fast orientations have a circular mean value of 45.0° ± 41.1° and the splitting times range from 0.30 to 2.15 s with an average of 1.06 ± 0.32 s, which matches well with the global average of 1.0 s for continents (Silver, 1996).

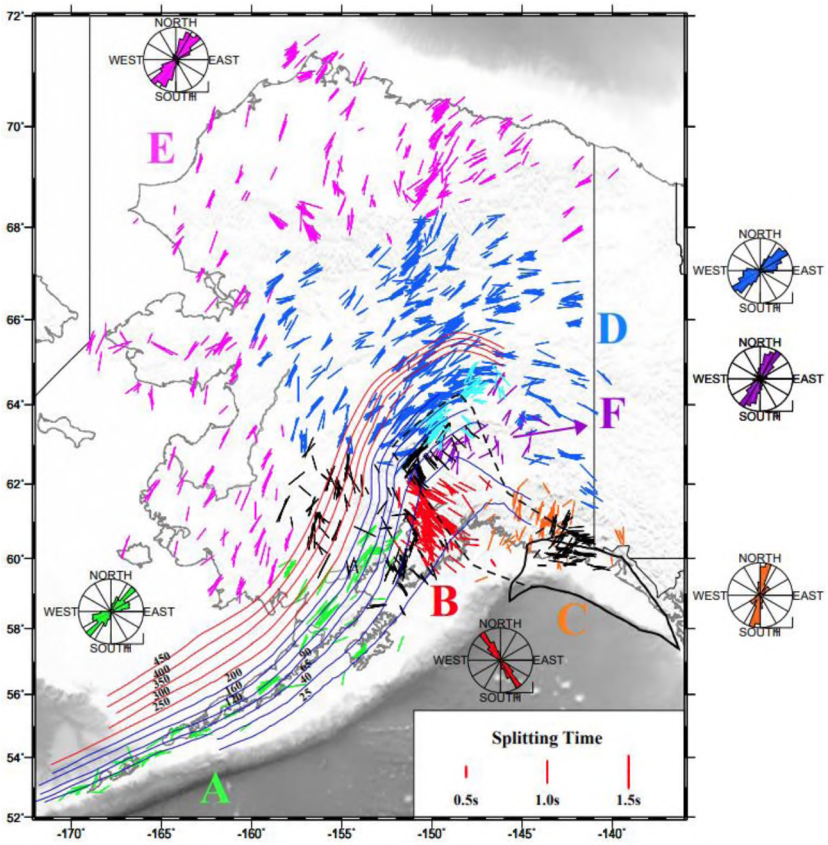

Figure 4. 2790 pairs of XKS splitting measurements from this study. Different colors represent measurements in six different sub-regions (except for the cyan bars). The values are plotted at the surface projections of the ray-piercing points at the depth of 200 km. Black and cyan bars represent results with azimuthal variations. The orientation of the bars represents the fast orientation, and the length is proportional to the splitting time.

The individual and station-averaged XKS measurements are respectively shown in Figures 4 and 5. Based on the different characteristics of the spatial distribution of the observed XKS splitting parameters, we divide the study area into six subregions (Figure 4). Note that some of the measurements showing a feature of complex anisotropy are marked as black bars in Figure 4, which are not included in the calculation of the mean splitting parameters for each of the areas and will be discussed in Section 4.3. The average fast orientation and splitting time of local S measurements are 62.4° ± 38.3° and

0.41 ± 0.20 s, respectively. Based on different splitting patterns, the local S results are divided into different groups in three regions (Figure 6).

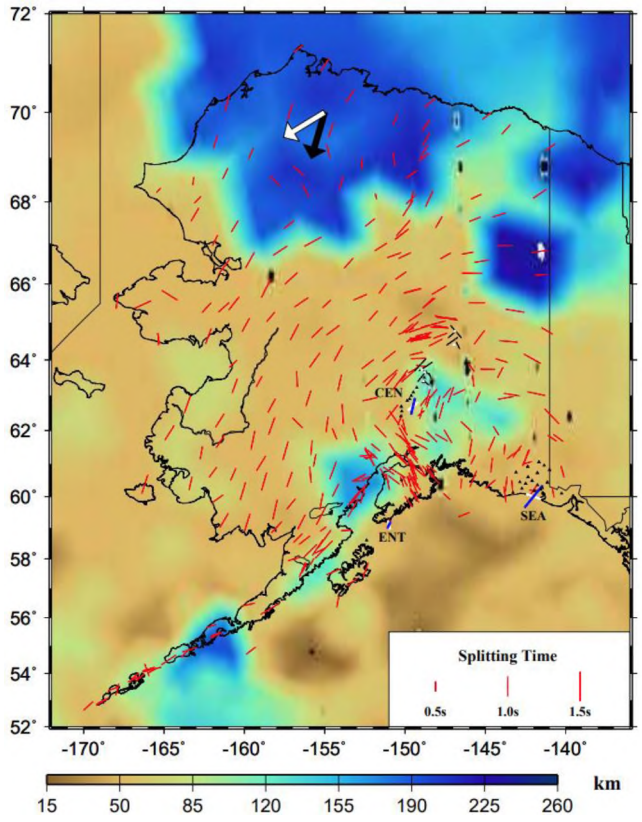

Figure 5. Station-averaged XKS splitting measurements. Red bars indicate the mean splitting measurements from each station that shows a simple anisotropy feature. Three regions of two-layered anisotropy are marked with names. White bars indicate the splitting parameters in upper layers and blue bars represent those in lower layers. Black dots mark stations whose results are combined for grid-searching for two-layered anisotropy in each region. Black bars are the average measurements from each group of measurements of the station showing spatially varying anisotropy. The background color represents the lithospheric thickness (Pasyano et al., 2014).

4.1. XKS MEASUREMENTS

4.1.1. Area A. Area A includes the Aleutian Islands, Kodiak Island and their adjacent areas (Figure 1) in the southwestern corner of Alaska where the Pacific slab

subducts beneath the Aleutian Arc with a relatively larger dip angle. This region contains 134 XKS measurements recorded at 53 stations and the fast orientations are dominantly trench-parallel with a circular mean of 50.8° ± 21.5° (Figure 4). The mean splitting time is 1.04 ± 0.32 s in which the highest value emerges around ~158° W. In this area, two of the previous studies (McPherson et al., 2020; Venereau et al., 2019) reported a comparable number of SWS measurements which are largely consistent with our results.

4.1.2. Area B. Area B is situated in southcentral Alaska including the Kenai Peninsula and the western part of the Yakutat terrane (Figure 1). It is separated from Area A by an along-trench abrupt change in the fast orientations, from trench-parallel to trench-perpendicular, with a circular mean of 145.9° ± 17.1° (Figure 4) and a mean splitting time of 1.06 ± 0.30 s. This area contains 345 measurements from 49 stations, and the results are consistent with previous SWS studies (Hanna & Long., 2012; Perttu et al., 2014; Venereau et al., 2019; McPherson et al., 2020).

4.1.3. Area C. Area C locates in the southeastern corner of Alaska and is characterized by the collision between the unsubducted portion of the Yakutat terrane and southeastern Alaska (Figure 1), referred to as Yakutat collision zone (McPherson et al., 2020). A total of 75 measurements obtained at 21 stations in this area show the feature of simple anisotropy, while those obtained at the other 27 stations are characterized by systematic azimuthal variations indicative of complex anisotropy. Most of the simple anisotropy results exist in the western part of the area and show NNE-SSW to N-S fast orientations (Figure 4).

4.1.4. Area D. Area D includes most of the regions between the Alaska Range (AR) and Brooks Range (Figure 1). It is distinguished from other areas in that the

splitting parameters in this region show a circular pattern, which is approximately centered at 147°W and 63°N, a possible location of the slab edge proposed by several previous studies (Gou et al., 2019; Hanna & Long, 2012; Venereau et al., 2019). The fast orientations from the 1172 measurements at 97 stations have a mean value of 57.8° ± 26.2° (Figure 4), while the corresponding splitting times have an average value of 1.11 ± 0.30 s.

4.1.5. Area E. Area E consists of the region north of the Brooks Range and most part of western Alaska including the Seward Peninsula (Figure 1). The fast orientations from 566 measurements at 72 stations have an average of 33.0° ± 27.3° (Figure 4), which is approximately consistent with the Apparent Plate Motion (APM) direction (Figure 1) in the HS3-NUVEL-1A model (Gripp & Gordon, 2002), and the mean splitting time is 1.01 ± 0.29 s. In addition, we observe two areas with anomalous NW-SE fast orientations centered approximately at (68°N, 157°E) and (65.5°N, 165°E), respectively. Such orientations are distinctively different from the surrounding measurements and possible formation mechanisms have not been discussed by previous studies.

4.1.6. Area F. Area F resides in the northeast part of the Yakutat slab and its nearby areas. This region contains 14 stations and is differentiated from Area B and Area D by showing dominant NNE-SSW fast orientations (Figure 4), with an average value of 25.8° ± 27.9°. The average splitting time is 0.98 ± 0.31s. Our results are consistent with those in the northwestern part of the "Slab Connection" region (McPherson et al., 2020). In addition, a large number of null measurements have been proposed in this region (Hanna & Long, 2012; McPherson et al., 2020).

4.2. LOCAL S MEASUREMENTS

4.2.1. Region 1. Region 1 includes the area west of ~163° of the Aleutian arc. This region contains 48 measurements from 21 seismic stations and no previous local S investigations have been conducted in this region. The measurements here are distinguished by their generally trench-normal fast orientations with a mean value of 138.8° ± 39.1° (Figure 6). The average splitting time is 0.42 ± 0.17 s.

4.2.2. Region 2. Region 2 locates in the area between ~163° and ~152° of the Aleutian arc. The region consists of 114 measurements obtained from 31 stations. The average splitting parameters are 60.3° ± 28.9° and 0.43 ± 0.26 s for the fast orientations and splitting times, respectively (Figure 6). A recent local S investigation exhibits uniform trench-parallel measurements in the forearc region and trench-perpendicular measurements in the backarc region (Karlowska et al., 2021). Our results are similar but we only obtain one measurement in the backarc region from a single station (SVW2).

4.2.3. Region 3. Region 3 locates in the area away from the Aleutian arc and includes the forearc and backarc regions in central Alaska (Figure 6). There are 85 measurements recorded from 18 stations and no previous local S splitting results are found in this region. Similar to the results in region 2, the measurements here are also characterized by trench-parallel fast orientations which have an average value of 60.3° ± 29.6°. The mean splitting time is 0.38 ± 0.13 s.

4.3. CHARACTERIZATION OF COMPLEX ANISOTROPY

4.3.1. Two-Layered Anisotropy. As the most common form of complex anisotropy, two-layered anisotropy is initially proposed by Silver and Savage (1994) and

the two pairs of splitting parameters can be determined using the grid-searching technique. Due to the non-uniqueness of the resulting optimal parameters (Gao et al., 2010; Hammond et al., 2014), several constraints have been applied to improve the reliability of the results.

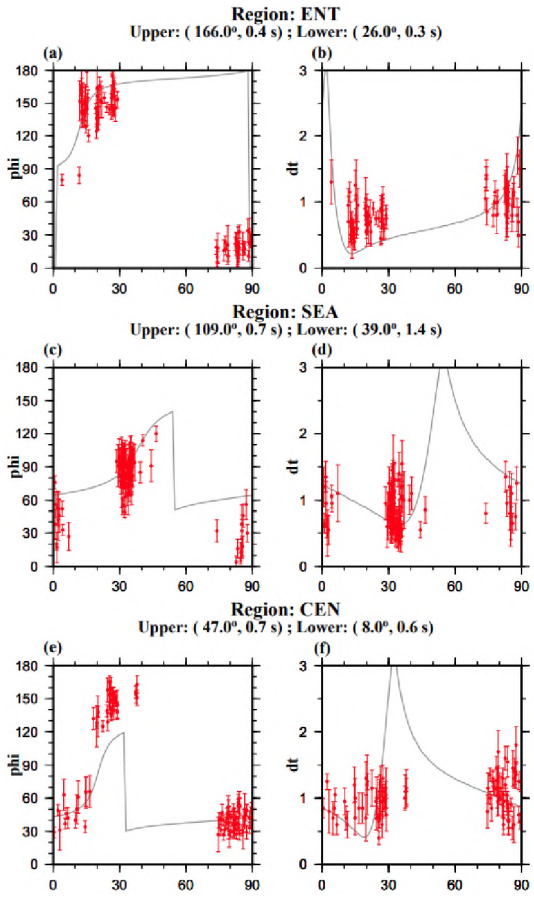

Figure 7. Azimuthal variations of the combined splitting parameters from three regions. The plots on the right are fast orientations against BAZ 90°, while those on the left are splitting times against BAZ 90°. Gray lines indicate the predicted splitting parameters.

For example, an assumption that the upper layer anisotropy is originated in the crust whose anisotropy properties are determined using receiver functions is made (Wu et al., 2015), and the splitting parameters from the lower layer is constrained by assuming

that the fast orientation is parallel to the asthenospheric flow (Yang et al., 2014). Another way to improve the reliability of the searched parameters is to combine results from nearby stations with similar splitting patterns (Cherie et al., 2016; Kong et al., 2018; Yang et al., 2014). Both of the aforementioned approaches are used in this study.

Through visually scrutinizing the splitting parameters of all the stations used in the study area, we search for the patterns of complex anisotropy, which is characterized by systematic azimuthal variations. Finally, three regions, respectively named CEN (Central Alaska), SEA (Southeastern Alaska), and ENT (Entrained Flow Region), are identified (Figures 5 and 7) as possessing a two-layered anisotropic structure and the stations with similar measurements in each region are combined. The three sets of combined measurements are then used to grid-search the optimal parameters according to the procedures detailed in Gao & Liu (2009), in which misfits are calculated and the weighting factors are designed for obtaining the optimal pairs of parameters (Gao & Liu, 2009).

Regions CEN and ENT exhibit a well-defined two-layered structure. However, the two-layered model is not well-contrained in region SEA, possibly related to the existence of intrinsic non-uniqueness. To provide the a priori constraint to reduce the non-uniqueness, we take a Bayesian approach by assuming that the anisotropy in the upper layer is generated in the lithosphere with a fast orientation in the range of 80° - 110°. Such an assumption is made based on the following reasons. First, several studies indicate that the anisotropy in region SEA may include the contribution from both lithosphere and asthenosphere due to the complicated azimuthal variation in the SWS results (McPherson et al., 2020; Venereau et al., 2019). Second, previous studies propose

that the lithospheric anisotropy may be generated by past compression events, leading to fast orientations that are perpendicular to the maximum horizontal shortening direction (Silver, 1996). Region SEA locates in the Yakutat collision zone (Figure 1) which is characterized by nearly N-S to NNE-SSW maximum strain direction as indicated by GPS data (Marechal et al., 2015), thus corresponding to a nearly E-W to WWN-EES fast orientation in the lithosphere. After adding this a priori constraint, the optimal two-layered parameters are obtained.

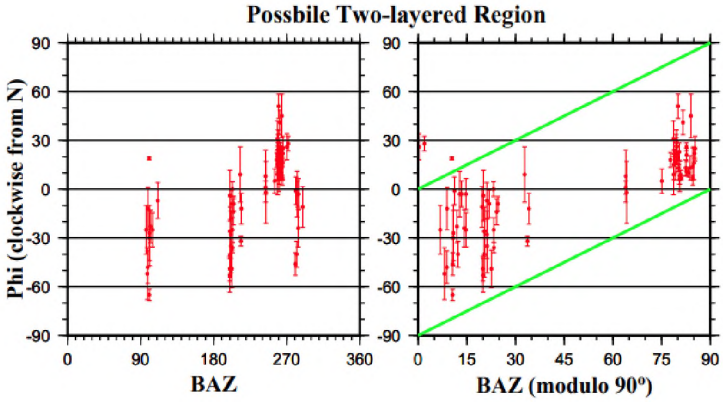

Figure 8. Splitting parameters for the possible two-layered region. The measurements are combined from results of 11 nearby stations.

Figure 7 shows the two-layered models with the corresponding parameters of the three regions. Region ENT locates in the western Kanai Peninsula (i.e. KP in Figure 1) and includes results from 6 individual stations. The combined individual parameters show a clear 90° periodicity (Figure 7a and 7b), indicating the existence of two-layered anisotropy. The fitted upper layer fast orientation is almost NW-SE (26°) and the lower layer's is NE-SW (166°). The splitting time for the upper and lower layers are 0.4 s and 0.3 s, respectively. Region SEA is in the southeast corner of Alaska and includes 27

stations showing a similar azimuthal variation (Figure 7c and 7d). The optimal parameters for the upper and lower layers are 47°, 0.7 s and 8°, 0.6 s, respectively. Region CEN includes 17 stations and is located near the 70 km slab depth contour line with an abrupt apparent fast orientation variation from NW-SE in the south to NE-SW in the north (Christenson & Abers, 2010).

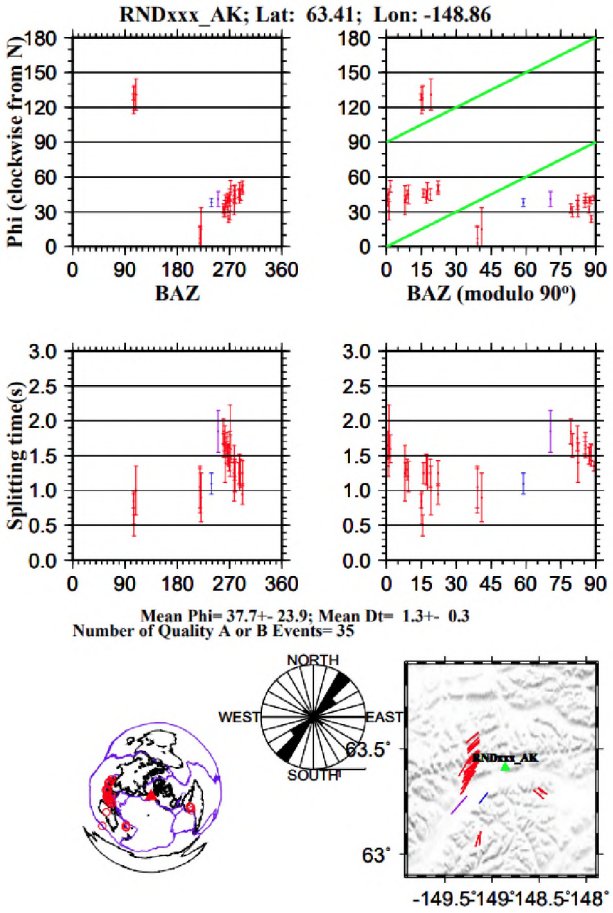

Figure 9. Example of spatially varying anisotropy. Coordinate graphs show splitting parameters against BAZ and BAZ 90°, respectively. Event location, rose diagram, and distribution of splitting parameters are shown in the bottom.

McPherson et al. (2020) indicate a similar region between the 50 and 100 km slab depth contour lines, where they observe strong azimuthal dependence in the splitting

parameters in which waves from northwest show NE-SW fast orientations and those from southeast produce NW-SE fast orientations, consistent with our individual measurements. However, the combined results show a strong azimuthal variation with a 90° periodicity (Figure 7e and 7f) that suggests a typical two-layered anisotropy. The resulting parameters for the upper and lower layers are 53°, 0.6 s and 13°, 0.8 s, respectively.

In the region where the strike of the subducting slab begins to divert into a nearly NNE-SSW direction (Figure 4), we find that the fast orientations are generally azimuthal dependent. We then combine similar results from 11 adjacent stations to increase the reliability (Figure 8). The measurements from west are dominantly within the range of 10° to 45°, consistent with the APM direction. On the other hand, most of the measurements from east and south are NW-SE or strike-parallel that are in accordance with those in Area B and Area A, respectively.

4.3.2. Spatially Varying Anisotropy. A special type of complex anisotropy, spatially varying anisotropy, is illustrated as presenting different splitting parameters for different seismic ray paths near the boundary of two or more areas. The splitting parameters vary according to ray-piercing locations and rarely demonstrate periodic azimuthal variations (e.g., Liu & Gao, 2013). In this study, the region possessing spatially varying anisotropy locates in the slab edge area and the corresponding measurements are marked as cyan bars (Figure 4).

These specific anisotropic patterns are seen in eight nearby stations which are subsequently combined together (Figure 10). As demonstrated by observations from RND, most of the events from southeast back azimuths show NW-SE fast orientations, while those from the west have NE-SW fast orientations (Figure 9).

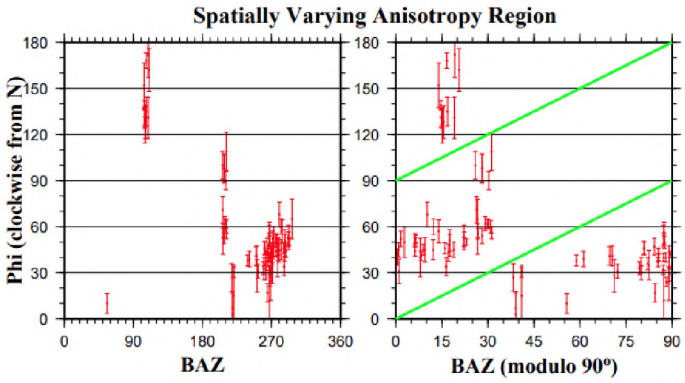

Figure 10. Fast orientation pattern against BAZ and BAZ 90° showing the existence of spatially varying anisotropy.

5. DISCUSSION

5.1. MANTLE FLOW SYSTEMS RESPONSIBLE FOR THE OBSERVED ANISOTROPY

5.1.1. Trench-Parallel Flow Beneath the Pacific Slab. Sub-slab trench-parallel flow has been proposed in numerous subduction zones to explain trench-parallel fast orientations (e.g., Russo and Silver, 1994). Long & Silver (2008) suggest that in the subslab region, anisotropy is dominantly controlled by 3D returned flow and is believed to be parallel to the trench, possibly generated by slab rollback associated with trench migration. The uniform trench-parallel XKS splitting fast orientations observed in the Aleutian arcs are consistent with the geometry of the Pacific slab imaged by previous tomography studies (Gou et al., 2019; Jiang et al., 2018; Martin-Short et al., 2018). However, the local S measurements in the Aleutian arcs show trench-parallel fast orientations only in region 2, while the fast orientations from local S splitting are nearly trench-normal in region 1 (Figure 6). Due to the fact that local S splitting represents the characteristic of mantle wedge anisotropy, the inconsistency between XKS and local S

results indicates that the uniform XKS trench-parallel measurements are originated from the sub-slab region. Similar interpretations are proposed by McPherson et al. (2020), in which they suggest that the thick Pacific slab separates the flows in the mantle wedge and the sub-slab region.

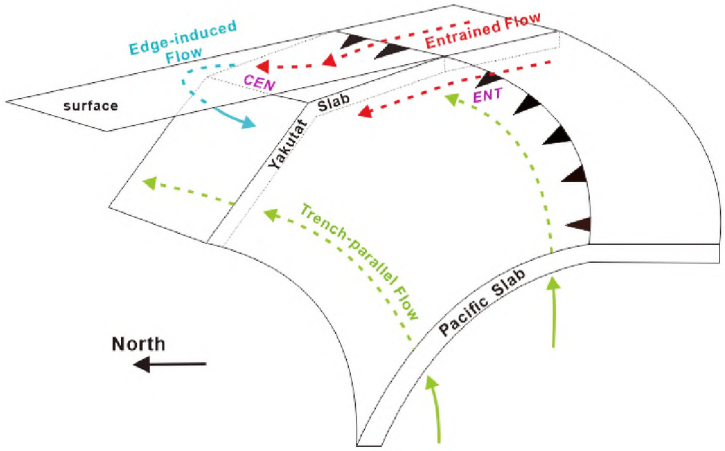

Figure 11. A three-dimensional mantle flow model of the Aleutian-Alaska subduction zone. Arrows with different colors represent mantle flows originated from different mechanisms. Black sawteeth mark the trench of the subduction zone. Purple texts (CEN and ENT) show the two-layered regions.

5.1.2. Entrained and Deflected Flow Beneath the Yakutat Slab. Another distinctly different mantle flow model, in which splitting fast orientations are trench-normal, refers to the flow entraining with the slab due to the viscous coupling between the subducting lithosphere and asthenosphere. Such mechanism has been proposed in several subduction zones, including Cascadia (Currie et al., 2004; Russo, 2009), Mexico-Rivera (León Soto et al., 2009), and the Peruvian segment of the Peru-Chile subduction zone (Eakin & Long, 2013). The northwestward insertion direction of the Yakutat slab is comparable to the trench-normal splitting orientations observed in the area, suggesting

the existence of an entrained flow system beneath the Yakutat slab. On the other hand, the local S results in this region are basically trench-parallel, indicative of a mantle wedge origin of the observed anisotropy. Such a contrast further suggests that the XKS splitting patterns mostly reflect subslab anisotropy associated with the trench-normal entrained flow system. Notably, the transition zone between Area A and Area B corresponds well with the two-layered region ENT (Figure 5). The 26° fast orientation in the lower layer (Figures 5 and 11) is consistent with the adjacent measurements along the eastern Aleutian arc, and the 166° fast orientation in the upper layer is also accord with the measurements for the Yakutat slab in Area B. Thus, we suggest that the two-layered anisotropic structure in this region is generated by the confluence of the two different mantle flow systems at different depths (Figure 11).

Unlike normal subducting situations with slabs plunging into the mantle, the slab of flat subductions commonly intrudes a few hundred kilometers horizontally, and then descends into the deeper mantle (Manea et al., 2017). Such geometrical feature also occurs on the Yakutat slab as demonstrated by the slab contour lines (Gou et al., 2019) in Figure 4. The Yakutat slab begins subducting with a steeper angle near the ~70 km slab depth contour line. This variation in slab geometry is corresponding to previous XKS results. Christensen & Abers (2010) indicate that in the area north of the 70 km contour line, the observed fast orientations are trench-parallel, while those south of the contour line are trench-normal, implying wedge-derived and subslab anisotropy, respectively. The conclusion generally agrees with ours; however, in our study, the identification of the two-layered anisotropy in region CEN (Figure 5) reveals an 8° fast orientation for the lower layer where the slab descends more steeply, possibly representing the flow

deflection. Such flow may further join the trench-parallel flow revealed by trench-parallel fast orientations in Area F. The 47° fast orientation for the upper layer is also consistent with the NE-SW fast orientation in Area D, indicating a mantle wedge origin. Therefore, we suggest that the region beneath the flat portion of the Yakutat slab is characterized by trench-normal entrained flow generated by the strong viscous coupling between the subducting lithosphere and asthenosphere. Beneath the steeply dipping portion of the slab, the flow gradually deflects to a trench-parallel direction probably due to the rollback of the steeply dipping slab (Olive et al., 2014; Paczkowski, et al., 2014a; Paczkowski, et al., 2014b).

5.1.3. Toroidal Flow Around the Slab Edge. Plentiful studies have observed the toroidal flow pattern associated with the slab edge effect (Civello & Margheriti, 2004; Eakin et al., 2010; Palano et al., 2017). They indicate that mantle materials may flow from one side to the other side of a slab around the edge due to three-dimensional mantle circulation. The Alaska subduction zone exhibits a typical slab edge (Figure 1), which has been imaged by numerous seismic tomography studies (Gou et al., 2019; Jiang et al., 2018; Martin-short et al., 2018). In addition, a toroidal flow model where the mantle materials are transferred from the subslab region into the mantle wedge has been proposed using geodynamic modeling (Jadamec & Billen, 2010, 2012). A circular pattern is observed in the proximity of 146°E, 64°N, the region of the proposed slab edge (Figures 4 and 5). We suggest that the circular pattern is induced by toroidal flow around the slab edge. Local S results in region 3 further indicate above-slab trench-parallel flow that is probably related to the low viscosity and high flux speed of this flow field

(Jadamec & Billen, 2012, 2013). Measurements from the adjacent Areas F and D may act as the beginning and final parts of the toroidal flow.

5.1.4. APM-Induced and Keel-Deflected Flow in Northern Alaska. The fast orientations in Area E are mostly parallel to the APM direction of the North American plate in both the NNR-MORVEL56 and Hotspot (Argus et al., 2011; Gripp & Gordon, 2002) models, and can be explained by the partial coupling between the asthenosphere and the overlying lithosphere. However, some NW-SE fast orientations, which are approximately normal to the APM direction, are found in the western Brooks Range and the Seward Peninsula (Figure 4). Such anomalously abrupt fast orientation changes have not been interpreted in previous SWS investigations in the study area but similar observations have been revealed and discussed in other regions. For instance, Klosko et al. (2001) observe fast orientations that shows a nearly 90° difference from those obtained at nearby stations which display APM-parallel fast orientations in the Ontong-Java oceanic plateau. They interpret this change as being affected by the distinct lithospheric root, which may have deflected the asthenospheric flow (Klosko et al., 2001). Likewise, the region where NW-SE fast orientations are observed coincides well with the highest elevation of the Brooks Range that corresponds to a deep continental root (Jiang et al., 2018; O'Driscoll & Miller, 2015). Thus, we suggest those measurements may be attributable to the deflection of APM-induced mantle flow system by the deep continental keel, although whether such a deep root exists beneath the Seward Peninsula is not clear. These mechanisms have been proposed in other regions with a rapid change in lithospheric thickness such as around the southern and eastern

margins of the North American Craton (Fouch & Rondenay, 2006; Refayee et al., 2014; Yang et al., 2017).

5.1.5. 3-D Dynamic Flow Model of the Subduction Zone. A three-dimensional model (Figure 11) of the spatial distribution of the anisotropy beneath Aleutian-Alaska subduction zone (Area A and Area B) is constructed to concisely present a multiple mantle flow system, which mainly consists of flows induced by three different mechanisms. The entrained mantle flow subducts beneath the flat portion of the Yakutat slab in a trench-perpendicular direction, possibly related to the viscous coupling between the subducting lithosphere and asthenosphere. Beneath the steeply dipping slab portion, it gradually diverts and moves toward the slab edge. The flow then spins around the slab edge, transfers sub-slab materials into the mantle wedge, resulting in an anticlockwise toroidal flow pattern (Figures 4 and 11). In the Aleutian arcs, sub-slab trench-parallel flow migrates along the steeply dipping Pacific slab due to the effect of slab rollback.

5.2. POSSIBLE UNDERGROUND STRUCTURES AND THEIR IMPLICATIONS

The SWS measurements have revealed different mantle flow systems throughout the entire Alaska region; however, several underground structures with complicated splitting patterns near the tectonic boundaries are still equivocal and opens to a variety of interpretations. Hence, we compare our results with previously proposed structures and discuss reasonable scenarios that may exist.

5.2.1. Possible Two-Layered Anisotropic Region. In the region where the slab strike turns into a nearly NNE-SSW direction, we observe numerous azimuthally dependent XKS measurements from 11 stations, possibly associated with the existence of

two-layered anisotropy. McPherson et al. (2020) obtain similar results of which the measurements from western back azimuths exhibit APM-parallel fast orientations, while those from south to southwest show fast orientations parallel to the slab strike, indicating the anisotropy from mantle wedge and sub-slab region, respectively. Unfortunately, due to the limited azimuthal coverage, we are not able to obtain a two-layered model from each of the 11 stations. Meanwhile, the combination of the 11 stations leads to another problem: the combination of the strike-parallel and NW-SE fast orientations in the assumed lower layer has resulted in the "overlapping phenomenon" of the fast orientations in BAZ 90° (Figure 8). Thus, we cannot grid-search the optimal splitting parameters for the two layers using combined data and such region is expected to be detected in future studies with more data.

Mountain Spurr (MS) (Figure 1) locates to the southeast of the possible two-layered region. This region is also featured by elusive splitting parameters from 6 stations. Similarly, each of these stations only shows a small number of measurements with different splitting parameters, which are lack of systematic azimuthal patterns and cannot be explained by either two-layered anisotropy or spatially varying anisotropy. Notably, the region is situated at the joint point of Area A and Area B, a tectonic transition zone that may account for the complicated splitting pattern (McPherson et al., 2020).

5.2.2. Possible Lithosphere Anisotropy in the Yakutat Collision Zone. The southeastern corner of Alaska has collided with the unsubducted potion of the Yakutat terrane (Figure 1) since mid-Miocene (Plafker & Berg, 1994). This region includes numerous E-W and NE-SW measurements, similar to those obtained from McPherson et

al. (2020). The combination of these similar results from 27 stations shows a clear azimuthal variation, suggesting the presence of a two-layered anisotropic structure (Figure 7c and 7d). Silver (1996) propose that lithospheric anisotropy can be generated by past compression activities, leading to fast orientations perpendicular to the maximum shortening direction. Therefore, the following assumption may account for the complicated splitting pattern here. The 109° fast orientation in the upper layer is perpendicular to the regional N-S to NNE-SSW maximum shortening direction (Marechal et al., 2015) and may stand for lithospheric anisotropy generated by the collision with the unsubducted Yakutat terrane. The 39° fast orientation in the lower layer is approximately consistent with the NNE-SSW measurements in Area C (Figure 4). We suggest that this lower layer anisotropy may stand for the asthenospheric mantle flow escaping from the Yakutat terrane or simply represent the APM-parallel anisotropy. Thus, a two-layered anisotropic model with a lithospheric upper layer on top of a 39° asthenospheric mantle flow layer is suggested in this region.

5.2.3. Formation Mechanism of the WVF. The WVF locates to the east of the Yakutat slab (Figure 1) and the volcanoes in this area are differentiated from Aleutian arc volcanoes by their atypical magmatic composition and controversial magma origin (Preece & Hart, 1994). In spite of the abrupt termination of the Wadati-Benioff zone at ~148°, a tectonic tremor study (Wech, 2016) argues that the Wrangell slab is likely aseismic due to the high tremor frequency in the vicinity of the WVF. Martin-Short et al., (2018) indicate that the Yakutat LAB ends directly beneath the WVF according to the surface wave tompgraphy results, while others image a high-velocity structure beneath the WVF, indicating the possible existence of a Wrangell slab (Gou et al., 2019; Jiang et

al., 2018; Yang & Gao, 2020). Our results show two anisotropic patterns in the proximity of the WVF: the dominant N-S trend of fast orientations in the western part of Area C and the circular trend in Area F. If the Wrangell slab does exist, the N-S fast orientation may represent another northward entrained flow beneath the Yakutat terrane. The difference in the direction between this flow and that in Area B may be associated with the varying geometry of the Yakutat slab. Alternatively, the WVF is possibly induced by the toroidal flow around the slab edge. This interpretation is further buttressed by numerous null measurements in the WVF region from other SWS studies (Hanna & Long, 2012; Mcpherson et al., 2020) and the existence of vertical upwelling suggested by geodynamic modelling studies (Jadamec & Billen, 2010; 2012). In this scenario, the N-S fast orientations to the south of the WVF likely represent the escaped flow moving through the Yakutat slab window, similar to the lower layer in the Yakutat collision zone.

6. CONCLUSIONS

To identify different mantle flow systems and probe relevant anisotropy structures beneath the entire Alaska region, a total of 2790 pairs of XKS and 247 pairs of local S splitting parameters are measured. Such unprecedented number of SWS measurements obtained using three seismic phases led to new understandings on regional mantle dynamics. Complex anisotropy is quantified in three regions in and near the subduction zone. The anisotropy structure in region ENT represents the confluence of different flow systems at different depths. Region SEA shows a two-layered structure that consists of a lower asthenospheric flow possibly escaped from the Yakutat slab window or induced by

the APM, under the assumption of an upper compression-induced anisotropic layer in the lithosphere. Region CEN exhibits two anisotropic layers, corresponding to the trench-parallel wedge flow and sub-slab entrained flow, respectively. The anisotropy structure in region ENT represents the confluence of different flow systems at different depths. The mantle flow mechanism in the Aleutian-Alaska subduction zone is highly varied and is mostly controlled by slab geometry and subducting approach. Beneath the normal-dipping Pacific slab, the mantle flow is dominantly trench-parallel. Under the flat Yakutat slab portion, the flow initially entrains with the slab and subsequently deflects to a trench-parallel direction, and moves toward the slab edge, generating anticlockwise toroidal flow therein. Finally, in the stable continental region away from the areas affected by the subduction, the observed anisotropy is mostly caused by APM-induced simple shear, with possible deflections induced by the deep continental keel.

REFERENCES

Argus, D. F., Gordon, R. G., & DeMets, C. (2011). Geologically current motion of 56 plates relative to the no-net-rotation reference frame. Geochemistry, Geophysics, Geosystems, 12(11), 1–13. https://doi.org/10.1029/2011GC003751

Bauer, M. A., Pavlis, G. L., & Landes, M. (2014). Subduction geometry of the Yakutat terrane, southeastern Alaska. Geosphere, 10(6), 1161–1176. https://doi.org/10.1130/GES00852.1

Becker, T. W., & Faccenna, C. (2009). A Review of the Role of Subduction Dynamics for Regional and Global Plate Motions. https://doi.org/10.1007/978-3-540-87974-9_1

Chastel, Y. B., Dawson, P. R., Wenk, H. R., & Bennett, K. (1993). Anisotropic convection with implications for the upper mantle. Journal of Geophysical Research, 98(B10), 17575–17771.

Cherie, S. G., Gao, S. S., Liu, K. H., Elsheikh, A. A., Kong, F., Reed, C. A., & Yang, B. B. (2016). Implications of complex seismic anisotropy. Geochemistry, Geophysics, Geosystems, 1975–1989. https://doi.org/10.1002/2016GC006269

Christensen, D. H., & Abers, G. A. (2010). Seismic anisotropy under central Alaska from SKS splitting observations. Journal of Geophysical Research, 115(B4), 1–12. https://doi.org/10.1029/2009jb006712

Christeson, G. L., Gulick, S. P. S., van Avendonk, H. J. A., Worthington, L. L., Reece, R. S., & Pavlis, T. L. (2010). The Yakutat terrane: Dramatic change in crustal thickness across the transition fault, Alaska. Geology, 38(10), 895–898. https://doi.org/10.1130/G31170.1

Civello, S., & Margheriti, L. (2004). Toroidal mantle flow around the Calabrian slab (Italy) from SKS splitting. Geophysical Research Letters, 31(10), 2001–2004. https://doi.org/10.1029/2004GL019607

Currie, C. A., Cassidy, J. F., Hyndman, R. D., & Bostock, M. G. (2004). Shear wave anisotropy beneath the Cascadia subduction zone and western North America craton. Geophysical Journal International, 157(1), 341–353. https://doi.org/10.1111/j.1365-246X.2004.02175.x

DeMets, C., Gordon, R. G., & Argus, D. F. (2010). Geologically current plate motions. Geophysical Journal International, 181(1), 1–80. https://doi.org/10.1111/j.1365-246X.2009.04491.x

Eakin, C. M., & Long, M. D. (2013). Complex anisotropy beneath the Peruvian flat slab from frequency-dependent, multiple-phase shear wave splitting analysis. Journal of Geophysical Research E: Planets, 118(9), 4794–4813. https://doi.org/10.1002/jgrb.50349

Eakin, C. M., Obrebski, M., Allen, R. M., Boyarko, D. C., Brudzinski, M. R., & Porritt, R. (2010). Seismic anisotropy beneath Cascadia and the Mendocino triple junction: Interaction of the subducting slab with mantle flow. Earth and Planetary Science Letters, 297(3–4), 627–632. https://doi.org/10.1016/j.epsl.2010.07.015

Eberhart-Phillips, D., Christensen, D. H., Brocher, T. M., Hansen, R., Ruppert, N. A., Haeussler, P. J., & Abers, G. A. (2006). Imaging the transition from Aleutian subduction to Yakutat collision in central Alaska, with local earthquakes and active source data. Journal of Geophysical Research: Solid Earth, 111(11), 1–31. https://doi.org/10.1029/2005JB004240

Finzel, E. S., Trop, J. M., Ridgway, K. D., & Enkelmann, E. (2011). Upper plate proxies for flat-slab subduction processes in southern Alaska. Earth and Planetary Science Letters, 303(3–4), 348–360. https://doi.org/10.1016/j.epsl.2011.01.014

Fisher, M. A., & Magoon, L. B. (1978). Geologic framework of lower Cook Inlet, Alaska. AAPG Bulletin (American Association of Petroleum Geologists), 62(3), 373–402. https://doi.org/10.1306/c1ea4851-16c9-11d7-8645000102c1865d

Fouch, M. J., & Fischer, K. M. (1996). Mantle anisotropy beneath northwest Pacific subduction zones. Journal of Geophysical Research B: Solid Earth, 101(B7), 15987–16002. https://doi.org/10.1029/96jb00881

Fouch, M. J., & Rondenay, S. (2006). Seismic anisotropy beneath stable continental interiors. Physics of the Earth and Planetary Interiors, 158(2–4), 292–320. https://doi.org/10.1016/j.pepi.2006.03.024

Francis, T. J. G. (1969). Generation of seismic anisotropy in the upper mantle along the mid-ocean ridges. Nature, 221, 177–178. Retrieved from http://adsabs.harvard.edu/abs/1969Natur.224..177K

Gao, S., Davis, P. M., Liu, H., Slack, P. D., Rigor, A. W., Zorin, Y. A., et al. (1997). SKS splitting beneath continental rift zones. Journal of Geophysical Research: Solid Earth, 102(B10), 22781–22797. https://doi.org/10.1029/97jb01858

Gao, S. S., & Liu, K. H. (2009). Significant seismic anisotropy beneath the southern Lhasa Terrane, Tibetan Plateau. Geochemistry, Geophysics, Geosystems, 10(2), 1–19. https://doi.org/10.1029/2008GC002227

Gao, S. S., Liu, K. H., & Abdelsalam, M. G. (2010). Seismic anisotropy beneath the Afar Depression and adjacent areas: Implications for mantle flow. Journal of Geophysical Research: Solid Earth, 115(12), 1–15. https://doi.org/10.1029/2009JB007141

Gou, T., Zhao, D., Huang, Z., & Wang, L. (2019). Aseismic deep slab and mantle flow beneath Alaska: Insight from anisotropic tomography. Journal of Geophysical Research: Solid Earth, 124(2), 1700–1724. https://doi.org/10.1029/2018JB016639

Gripp, A. E., & Gordon, R. G. (2002). Young tracks of hotspots and current plate velocities. Geophysical Journal International, 150(2), 321–361. https://doi.org/10.1046/j.1365-246X.2002.01627.x

Hall, C. E., Fischer, K. M., Parmentier, E. M., & Blackman, D. K. (2000). The influence of plate motions on three-dimensional back arc mantle flow and shear wave splitting. Journal of Geophysical Research: Solid Earth, 105(B12), 28009–28033. https://doi.org/10.1029/2000jb900297

Hammond, J. O. S., Kendall, J.-M., Wookey, J., Stuart, G. W., Keir, D., & Ayele, A. (2014). Differentiating flow, melt, or fossil seismic anisotropy beneath Ethiopia. Geochemistry, Geophysics, Geosystems, 15, 1878–1894. https://doi.org/10.1002/2013GC005185.

Hanna, J., & Long, M. D. (2012). SKS splitting beneath Alaska: Regional variability and implications for subduction processes at a slab edge. Tectonophysics, 530–531, 272–285. https://doi.org/10.1016/j.tecto.2012.01.003

Hess, H. H. (1964). Seismic Anisotropy of the Uppermost Mantle under Oceans. Nature, 203(4945), 629–631.

Jadamec, M. A., & Billen, M. I. (2010). Reconciling surface plate motions with rapid three-dimensional mantle flow around a slab edge. Nature, 465, 338–341. https://doi.org/https://doi.org/10.1038/nature09053

Jadamec, M. A., & Billen, M. I. (2012). The role of rheology and slab shape on rapid mantle flow: Three-dimensional numerical models of the Alaska slab edge. Journal of Geophysical Research: Solid Earth, 117(2), 1–20. https://doi.org/10.1029/2011JB008563

Jiang, C., Schmandt, B., Ward, K. M., Lin, F. C., & Worthington, L. L. (2018). Upper mantle seismic structure of Alaska from Rayleigh and S wave tomography. Geophysical Research Letters, 45(19), 10,350-10,359. https://doi.org/10.1029/2018GL079406

Karato, S., Jung, H., Katayama, I., & Skemer, P. (2008). Geodynamic significance of seismic anisotropy of the upper mantle: New insights from laboratory studies. Annual Review of Earth and Planetary Sciences, 36, 59–95. https://doi.org/10.1146/annurev.earth.36.031207.124120

Karlowska, E., Bastow, I. D., Rondenay, S., Martin-Short, R., & Allen, R. M. (2021). The development of seismic anisotropy below south-central Alaska: evidence from local earthquake shear wave splitting. Geophysical Journal International, 225(1), 548–554. https://doi.org/10.1093/gji/ggaa603

Klosko, E. R., Russo, R. M., Okal, E. A., & Richardson, W. P. (2001). Evidence for a rheologically strong chemical mantle root beneath the Ontong-Java Plateau. Earth and Planetary Science Letters, 186(3–4), 347–361. https://doi.org/10.1016/S0012-821X(01)00235-7

Kong, F., Wu, J., Liu, L., Liu, K. H., Song, J., Li, J., & Gao, S. S. (2018). Azimuthal anisotropy and mantle flow underneath the southeastern Tibetan Plateau and northern Indochina Peninsula revealed by shear wave splitting analyses. Tectonophysics, 747–748(May), 68–78. https://doi.org/10.1016/j.tecto.2018.09.013

León Soto, G., Ni, J. F., Grand, S. P., Sandvol, E., Valenzuela, R. W., Guzmán Speziale, M., et al. (2009). Mantle flow in the Rivera-Cocos subduction zone. Geophysical Journal International, 179(2), 1004–1012. https://doi.org/10.1111/j.1365-246X.2009.04352.x

Liu, K. H., & Gao, S. S. (2013). Making reliable shear-wave splitting measurements. Bulletin of the Seismological Society of America, 103(5), 2680–2693. https://doi.org/10.1785/0120120355

Long, M. D., & Becker, T. W. (2010). Mantle dynamics and seismic anisotropy. Earth and Planetary Science Letters, 297(3–4), 341–354. https://doi.org/10.1016/j.epsl.2010.06.036

Long, M. D., & Silver, P. G. (2008). The subduction zone flow field from seismic anisotropy: A global view. Science, 319(5861), 315–318. https://doi.org/10.1126/science.1150809

Long, M. D., & Silver, P. G. (2009). Shear wave splitting and mantle anisotropy: Measurements, interpretations, and new directions. Surveys in Geophysics, 30(4–5), 407–461. https://doi.org/10.1007/s10712-009-9075-1

Long, M. D., & Wirth, E. A. (2013). Mantle flow in subduction systems: The mantle wedge flow field and implications for wedge processes. Journal of Geophysical Research: Solid Earth, 118(2), 583–606. https://doi.org/10.1002/jgrb.50063

Manea, V. C., Manea, M., Ferrari, L., Orozco, T., Valenzuela, R. W., Husker, A., & Kostoglodov, V. (2017). A review of the geodynamic evolution of flat slab subduction in Mexico, Peru, and Chile. Tectonophysics, 695, 27–52. https://doi.org/10.1016/j.tecto.2016.11.037

Marechal, A., Mazzotti, S., Elliott, J. L., Freymueller, J. T., & Schmidt, M. (2015). Indentor-corner tectonics in the Yakutat-St. Elias collision constrained by GPS. Journal of Geophysical Research: Solid Earth, 120, 3897–3908. https://doi.org/10.1002/2014JB011842

Martin-Short, R., Allen, R., Bastow, I. D., Porritt, R. W., & Miller, M. S. (2018). Seismic imaging of the Alaska subduction zone: Implications for slab geometry and volcanism. Geochemistry, Geophysics, Geosystems, 19(11), 4541–4560. https://doi.org/10.1029/2018GC007962

McPherson, A. M., Christensen, D. H., Abers, G. A., & Tape, C. (2020). Shear wave splitting and mantle flow beneath alaska. Journal of Geophysical Research: Solid Earth, 125(4), 1–18. https://doi.org/10.1029/2019jb018329

O'Driscoll, L. J., & Miller, M. S. (2015). Lithospheric discontinuity structure in Alaska, thickness variations determined by Sp receiver functions. Tectonics, 34(4), 694–714. https://doi.org/10.1002/2014TC003669

Olive, J. A., Pearce, F., Rondenay, S., & Behn, M. D. (2014). Pronounced zonation of seismic anisotropy in the Western Hellenic subduction zone and its geodynamic significance. Earth and Planetary Science Letters, 391, 100–109. https://doi.org/10.1016/j.epsl.2014.01.029

Paczkowski, K., Thissen, C. J., Long, M. D., & Montési., L. G. J. (2014). Deflection of mantle flow beneath subducting slabs and the origin of subslab anisotropy. Geophysical Research Letters, 41(April), 6734–6742. https://doi.org/10.1002/2014GL060914.

Paczkowski, K., Montési., L. G. J., Long, M. D., & Thissen, C. J. (2014). Three-dimensional flow in the subslab mantle. Geochemistry, Geophysics, Geosystems, 15, 3989–4008. https://doi.org/10.1002/ 2014GC005441.

Palano, M., Piromallo, C., & Chiarabba, C. (2017). Surface imprint of toroidal flow at retreating slab edges: The first geodetic evidence in the Calabrian subduction system. Geophysical Research Letters, 44(2), 845–853. https://doi.org/10.1002/2016GL071452

Perttu, A., Christensen, D., Abers, G., & Song, X. (2014). Insights into mantle structure and flow beneath Alaska based on a decade of observations of shear wave splitting. Journal of Geophysical Research, Solid Earth, 119, 8366–8377. https://doi.org/10.1002/ 2014JB011359.

Plafker, G., & Berg, H. (1994). The geology of Alaska. Overview of the geology and tectonic evolution of Alaska, The geology of North America series (Vol. G - 1, pp. 989 - 1021). America: Geological Society.

Preece, S. J., & Hart, W. K. (2004). Geochemical variations in the <5 Ma Wrangell Volcanic Field, Alaska: Implications for the magmatic and tectonic development of a complex continental arc system. Tectonophysics, 392(1–4), 165–191. https://doi.org/10.1016/j.tecto.2004.04.011

Qi, C., Zhao, D., & Chen, Y. (2007). Search for deep slab segments under Alaska. Physics of the Earth and Planetary Interiors, 165(1–2), 68–82. https://doi.org/10.1016/j.pepi.2007.08.004

Rasendra, N., Bonnin, M., Mazzotti, S., & Tiberi, C. (2014). Crustal and upper-mantle anisotropy related to fossilized transpression fabric along the denali fault, Northern Canadian Cordillera. Bulletin of the Seismological Society of America, 104(4), 1964–1975. https://doi.org/10.1785/0120130233

Refayee, H. A., Yang, B. B., Liu, K. H., & Gao, S. S. (2014). Mantle flow and lithosphere-asthenosphere coupling beneath the southwestern edge of the North American craton: Constraints from shear-wave splitting measurements. Earth and Planetary Science Letters, 402(C), 209–220. https://doi.org/10.1016/j.epsl.2013.01.031

Russo, R. M. (2009). Subducted oceanic asthenosphere and upper mantle flow beneath the Juan de Fuca slab. Lithosphere, 1(4), 195–205. https://doi.org/10.1130/L41.1

Russo, R. M., & Silver, P. G. (1994). Trench-parallel flow beneath the Nazca plate from seismic anisotropy. Science, 263(5150), 1105–1111. https://doi.org/10.1126/science.263.5150.1105

Savage, M. S. (1999). Seismic anisotropy and mantle deformation: What have we learned from shear wave splitting? Reviews of Geophysics, 37(1), 65–106. https://doi.org/10.1029/98RG02075

Schellart, W. P. (2004). Kinematics of subduction and subduction-induced flow in the upper mantle. Journal of Geophysical Research: Solid Earth, 109(7), 1–19. https://doi.org/10.1029/2004JB002970

Silver, P. G. (1996). Seismic anisotropy beneath the continents: Probing the depths of geology. Annual Review of Earth and Planetary Sciences, 24, 385–432. https://doi.org/10.1146/annurev.earth.24.1.385

Silver, P. G., & Chan, W. W. (1988). Implications for continental structure and evolution from seismic anisotropy. Nature, 335(6185), 34–39. https://doi.org/10.1038/335034a0

Silver, P. G., & Chan, W. W. (1991). Shear wave splitting and subcontinental mantle deformation. Journal of Geophysical Research, 96, 16429–16454. https://doi.org/10.1017/S0002020600023313

Silver, P. G., & Savage, M. K. (1994). The interpretation of shear-wave splitting parameters in the presence of two anisotropic layers. Geophysical Journal International, 119, 949–963. https://doi.org/10.2307/20001495

Stegman, D. R., Freeman, J., Schellart, W. P., Moresi, L., & May, D. (2006). Influence of trench width on subduction hinge retreat rates in 3-D models of slab rollback. Geochemistry, Geophysics, Geosystems, 7(3). https://doi.org/10.1029/2005GC001056

Vauchez, A., & Nicolas, A. (1991). Mountain building: strike-parallel motion and mantle anisotropy. Tectonophysics, 185(3–4), 183–201. https://doi.org/10.1016/0040-1951(91)90443-V

Venereau, C. M. A., Martin-Short, R., Bastow, I. D., Allen, R. M., & Kounoudis, R. (2019). The role of variable slab dip in driving mantle flow at the eastern edge of the Alaskan subduction margin: Insights from shear-wave splitting. Geochemistry, Geophysics, Geosystems, 20(5), 2433–2448. https://doi.org/10.1029/2018GC008170

Vinnik, L. P., Makeyeva, L. I., Milev, A., & Usenko, A. Y. (1992). Global patterns of azimuthal anisotropy and deformations in the continental mantle. Geophysical Journal International, 111(3), 433–447. https://doi.org/10.1111/j.1365-246X.1992.tb02102.x

Wang, Y., & Tape, C. (2014). Seismic velocity structure and anisotropy of the Alaska subduction zone based on surface wave tomography. Journal of Geophysical Research: Solid Earth, 119(12), 8845–8865. https://doi.org/10.1002/2014JB011438

Wech, A. G. (2016). Extending Alaska's plate boundary: Tectonic tremor generated by Yakutat subduction. Geology, 44(7), 587–590. https://doi.org/10.1130/G37817.1

Wu, J., Zhang, Z., Kong, F., Yang, B. B., Yu, Y., Liu, K. H., & Gao, S. S. (2015). Complex seismic anisotropy beneath western Tibet and its geodynamic implications. Earth and Planetary Science Letters, 413, 167–175. https://doi.org/10.1016/j.epsl.2015.01.002

Yang, B., Gao, S. S., Liu, K. H., Elsheikh, A. A., Lemnifi, A. A., Refayee, H. A., & Yu, Y. (2014). Seismic anisotropy and mantle flow beneath the northern Great Plains of North America. Journal of Geophysical Research: Solid Earth, 119(3), 1971–1985. https://doi.org/10.1002/2013JB010561

Yang, B. B., Liu, Y., Dahm, H., Liu, K. H., & Gao, S. S. (2017). Seismic azimuthal anisotropy beneath the eastern United States and its geodynamic implications. Geophysical Research Letters, 44(6), 2670–2678. https://doi.org/10.1002/2016GL071227

Yang, X., & Gao, H. (2020). Segmentation of the Aleutian-Alaska subduction zone revealed by full-wave ambient noise tomography: Implications for the along-strike variation of volcanism. Journal of Geophysical Research: Solid Earth, 125(11), 1–20. https://doi.org/10.1029/2020JB019677

Yang, X., Fischer, K. M., & Abers, G. A. (1995). Seismic anisotropy beneath the Shumagin Islands segment of the Aleutian-Alaska subduction zone. Journal of Geophysical Research, 100(B9), 18165–18177. https://doi.org/10.1029/95jb01425

Zhang, Z., & Karato, S. (1995). Lattice preferred orientation of olivine aggregates deformed in simple shear. Nature, 375, 774–777. https://doi.org/10.1038/375774a0

Zhao, D., Christensen, D., & Pulpan, H. (1995). Tomographic imaging of the Alaska subduction zone. Journal of Geophysical Research, 100(B4), 6487–6504. https://doi.org/10.1029/95JB00046

II. MANTLE FLOW IN THE VICINITY OF THE EASTERN EDGE OF THE PACIFIC-YAKUTAT SLAB: CONSTRAINTS FROM SHEAR WAVE SPLITTING ANALYSES

ABSTRACT

To investigate the effects of a slab edge and varying slab geometry on the mantle flow systems beneath south central Alaska, a total of 971 pairs of teleseismic shear wave (SKS, SKKS, and PKS) and 65 pairs of local S wave splitting parameters (fast orientations and splitting times) are measured using data from the USArray and other networks. The Pacific-Yakutat slab edge separates two regions with different characteristics of the splitting measurements. The area to the west of the slab edge has greater splitting times and mostly trench parallel fast orientations, and the area to the east is dominated by smaller splitting times and spatially varying fast orientations. The spatial distribution of the splitting parameters and results of anisotropy layering and depth analyses can be explained by a model involving three flow systems. The sub-slab flow initially entraining with the shallow-dipping Yakutat slab deflects to a trench-parallel direction near due to slab retreat and an increase in slab dip, and flows northeastward toward the slab edge, where it splits into two branches. The first branch enters the mantle wedge as a toroidal flow and flows southwestward along the slab, and the second branch continues approximately eastward. The flowlines of the toroidal and continued flow systems are approximately orthogonal to each other in the vicinity of the Pacific-Yakutat slab edge, producing the observed small splitting times and spatially varying fast orientations.

1. INTRODUCTION

The eastern terminus of the Pacific-Yakutat slab in south central Alaska (Figure 1) is characterized by the partial subduction of the Yakutat terrene (YT), which has its origin as an oceanic plateau with anomalous crust of more than 20 km thick (Christensen et al., 2010; Ferris et al., 2003; Worthington et al., 2012). The buoyancy of the subducted portion of the YT has led to flat and shallow subduction in the area from the trench to ~600 km inland (Eberhart-Phillips et al., 2006), where the slab resumes a steeper dip that is comparable to that of the neighboring normal oceanic slab (Figure 1). Slab rollback and southward trench migration of the "normal" Pacific slab west of the YT have been suggested by geodynamic modeling (Schellart et al., 2007), although the YT portion of the slab may not experience rollback due to its high buoyancy (Jadamec & Billen, 2012). Recent seismic tomography and receiver function studies suggest that the Pacific-Yakutat slab may plunge into a depth of over ~400 km in the mantle (Dahm et al., 2017; Gou et al., 2019; Jiang et al., 2018; Martin-Short et al., 2018). Seismic tomography studies reveal a sharp slab edge that is consistent with the eastward termination of the Wadati-Benioff zone (Martin-Short et al., 2018), while recent tomographic studies argue that the slab edge may extend further to the north in the area underlain by an aseismic section of the slab (Gou et al., 2019).

Numerous geodynamic modeling studies demonstrate that slab rollback near a slab edge can induce a toroidal component of mantle flow, which enters the mantle wedge from the sub-slab region (Jadamec & Billen, 2010, 2012; Kincaid & Griffiths, 2003; Stegman et al., 2006). Specifically for the study area in south central Alaska,

Jadamec & Billen (2012) conduct mantle flow modeling by considering a set of slab geometry ad rheology parameters. For virtually all models, an anticlockwise toroidal flow system associated with the Pacific-Yakutat slab edge is revealed. In contrast, based on azimuthal anisotropy measurements from the Moho to 200 km depth, a recent Rayleigh wave tomography study (Feng et al., 2020) suggests a clockwise flow system that continues toward the southeast after coming out from the slab edge.

One of the most effective techniques to provide direct constraints on mantle flow models is shear wave splitting (SWS) analysis (Hess, 1964; Silver & Chan, 1991). It has long been recognized that when a P-to-S converted wave from the core-mantle boundary (SKS, SKKS, and PKS, hereafter collectively called XKS) propagates through an azimuthally anisotropic layer, the shear wave would split into two components with orthogonally polarized directions and different traveling speeds (Ando, 1984; Silver & Chan, 1991). Two splitting parameters, the polarization orientation of the fast component (or fast orientation) and the arrival time difference between the fast and slow components (or splitting time), are measured to quantify the orientation and strength of the seismic azimuthal anisotropy, respectively.

The primary mechanism for the generation of seismic anisotropy in the upper mantle is the lattice preferred orientation (LPO) of the crystallographic axes of anisotropic minerals, especially olivine (Zhang & Karato, 1995). Under normal temperature and pressure conditions, progressive simple shear will result in the fast polarization orientation to be parallel to the a-axis of olivine (Ribe & Yu, 1991). Simple shear is commonly produced by the relative movements between the lithosphere and asthenosphere such as those associated with absolute plate motion and slab subduction

(Long & Becker, 2010; Schellart, 2004; Silver & Chan, 1991). Additionally, the a-axis aligns at a right angle to the direction of maximum horizontal compression under uniaxial compression (Ribe & Yu, 1991).

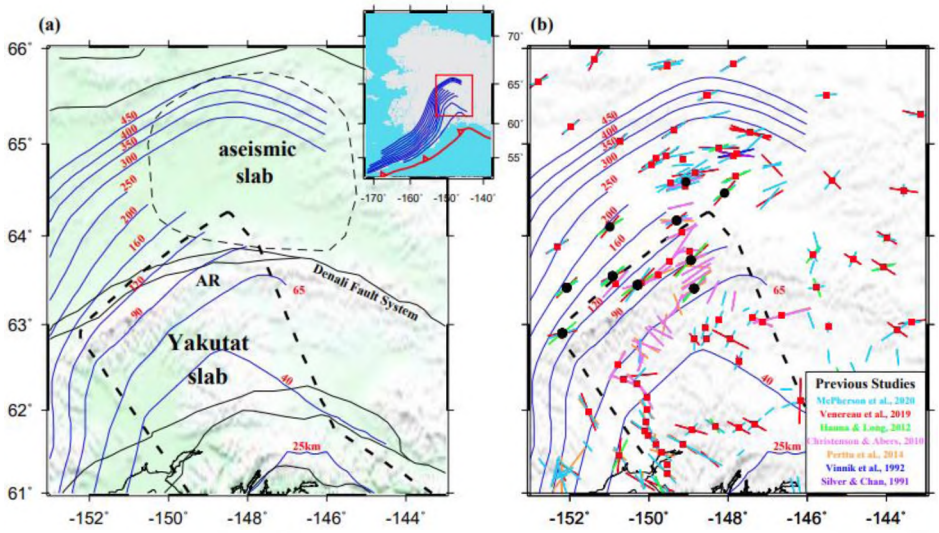

Figure 1. (a) Topographic relief map of the Alaska-Yakutat slab edge region with major geological structures. The Yakutat slab is delineated by the thick black dash line (Eberhart-Phillips et al., 2006), while the thin dash line indicates the aseismic slab area imaged by Gou et al. (2019). Contour lines of the depth of the Pacific slab are shown in blue (Gou et al., 2019). AR: Alaska Range. The upper right inset shows the location of the study area, which is outlined by a red rectangle. The red sawteeth mark the trench of the Alaska-Yakutat subduction zone. (b) Measurements from previous shear wave splitting studies labeled in the lower-right inset. Red squares and black dots mark the stations with XKS and local S measurements in this study, respectively.

In a subduction zone configuration, XKS splitting measurements mainly reflect the combined contributions from the mantle flows in the sub-slab region and the mantle wedge (Long & Silver, 2009; Perttu et al., 2014), although contributions from the slab and the lithosphere of the overriding plate cannot be completely excluded (Feng et al., 2020; Kong et al., 2020; Tian & Zhao, 2012). Trench-parallel flow in the sub-slab region is commonly attributed to slab rollback, which may also be responsible for trench-

perpendicular corner flow in the mantle wedge (e.g., Fouch & Fischer, 1996; Kong et al., 2020; Long & Silver, 2008, 2009; Russo & Silver, 1994). Away from the trench, trench-perpendicular entrained flow caused by viscous coupling between the slab and the underlying mantle has been proposed (Currie et al., 2004; Eakin & Long, 2013; Paczkowski et al., 2014; Russo & Silver, 1994). Numerous shear wave splitting measurements in the vicinity of a slab edge can be explained by edge induced toroidal flow (Civello & Margheriti, 2004; Hanna & Long, 2012; McPherson et al., 2020; Palano et al., 2017; Venereau et al., 2019).

Most XKS splitting studies including those conducted in Alaska (e.g., Christensen & Abers, 2010; Hanna & Long, 2012; Perttu et al., 2014; Venereau et al., 2019) were conducted under the assumption of simple anisotropy, which refers to anisotropy from a single anisotropic layer with a horizontal axis of symmetry (Silver & Chan, 1991). This ideal condition produces similar splitting parameters with respect to the arriving azimuth of the events (back-azimuth or BAZ). Departures from the ideal conditions of simple anisotropy are termed as complex anisotropy (Silver & Savage, 1994), and the most common form of complex anisotropy structure consists of two anisotropic layers, each with a horizontal axis of symmetry. The two-layered complex anisotropy is characterized by systematic azimuthal variations of the individual splitting parameters with a 90^{0} periodicity. Additionally, if a station is located near the boundary between two or more areas with different anisotropic characteristics, the observed anisotropy at the station may also vary azimuthally (referred to as spatially varying anisotropy hereinafter), although the variation may not necessarily possess a 90^{0} periodicity (Alsina & Snieder, 1995; Liu & Gao, 2013).

2. PREVIOUS SWS STUDIES AND RATIONALE OF THE PRESENT STUDY

A number of previous SWS studies have been carried out in the Alaska region (Figure 1b), elucidating some significant mantle flow features in the vicinity of the Pacific-Yakutat slab edge. The most prominent feature observed by pre-USArray studies (Christensen & Abers, 2010; Hanna & Long, 2012; Perttu et al., 2014) in this region is an ~90^0 change in the observed fast orientation near the ~70 km slab depth contour line, which separates the northern area with mostly trench-parallel fast orientations and the southern area that is dominated by trench-perpendicular orientations. The two clusters of fast orientations are mostly interpreted as reflecting along-strike flow in the mantle wedge and trench-perpendicular flow in the sub-slab region, respectively (Christensen & Abers, 2010).

Using data from some of the USArray and other stations, Venereau et al. (2019) and McPherson et al. (2020) conduct SWS investigations in the entire Alaska region. Both studies observe a circular pattern in the vicinity of the slab edge, and attribute the observations to an edge-induced toroidal flow system. Furthermore, on the basis of the consistency between the fast orientations and the strike of the regional strike-slip faults (e.g., Denali Fault, Figure 1a), the observed anisotropy near the fault zones is considered to be associated with shear strain generated by the relative motion along the faults (McPherson et al., 2020).

The current study was motivated by a number of factors. First, most of the previous SWS studies focus on identifying the different mantle flow systems in southern Alaska or the entire Alaska region (Hanna & Long, 2012; McPherson et al., 2020;

Venereau et al., 2019), and detailed analyses focused on the mantle flow systems associated with the slab edge are lacking. Second, complex anisotropy (mostly in the form of multi-layered anisotropy) has not been recognized in the study area due to a lack of adequate azimuthal coverage. Third, local S wave splitting analysis, which is an effective tool in discriminating wedge and sub-wedge anisotropy (e.g., Karlowska et al., 2021; Kong et al., 2020), is scarce in this region. Fourth, due to the vertical incidence of the XKS phases, the depth of the source of the observed XKS splitting remains ambiguous. Fifth, some aspects of the mantle flow systems in the slab edge region, including the lateral extent of the toroidal flow and the existence or absence of an eastward continuation of the sub-slab flow after it comes out of the slab edge, are still not well understood (Feng et al., 2020; Hanna & Long, 2012; Jadamec & Billen, 2010; Venereau et al., 2019).

In this study, we take advantage of the recent significant improvement in both the station and azimuthal coverages in the study area as a result of the USArray deployment to systematically investigate the mantle flow system in the vicinity of the Pacific-Yakutat slab edge in south central Alaska.

We isolate contributions of sub-slab anisotropy from the entire anisotropy region to the observed SWS using local S wave splitting analysis, estimate the depth of the source of XKS splitting using a spatial coherency approach (Gao & Liu, 2012; Liu & Gao, 2011), grid-search the two pairs of splitting parameters under a two-layered model (Silver & Savage, 1994), and propose a new mantle flow model to explain the observed seismic anisotropy.

3. DATA AND METHODS

The XKS and local S data used in this study were recorded by 106 broadband seismic stations (Figure 1b) located in the area of 61-66° N and 153-143°W, covering a recording period of 30 years from late 1988 to October 2019. The epicentral distance range is 83°-180°, 95°-180°, and 120°-180° for SKS, SKKS, and PKS, respectively (Liu & Gao, 2013).

In comparison, the latest SWS study covering the study area (McPherson et al., 2020) used only the SKS phase in the distance range of 80°-140° recorded during the period of early 2010 to middle 2017. The seismic data were requested from the Incorporated Research Institutions for Seismology (IRIS) Data Management Center (DMC).

The splitting parameters were measured and ranked following the procedures described in Liu & Gao (2013) for XKS and Jiang et al. (2021) for local S waves, and are briefly summarized below. For XKS splitting, the procedures were developed based on the minimization of transverse energy technique (Silver & Chan, 1991). Events with a magnitude of 5.6 or greater were used for data requesting from the DMC, and the cutoff magnitude was reduced to 5.5 for events with focal depths larger than 100 km.

For local S wave splitting analysis, the cutoff magnitude is 4.0. Additionally, only local events in the S-wave window (which is approximately within an angle of incidence of 35o) are used, and the splitting parameters were measured using the principle of minimizing the lesser of the two eigenvalues of the covariance matrix (Silver & Chan, 1991).

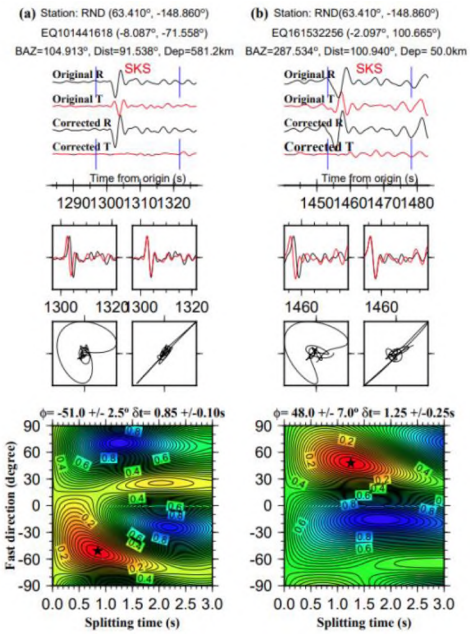

Figure 2. Examples of SWS measurements from two events recorded by station RND. The plots in the top row show original and corrected radial and transverse components, and plots in the central rows show the fast and slow waveforms and particle motions. The bottom plots are misfit maps, in which colors representing the energy on the corrected transverse component. The optimal pair of splitting parameters corresponds to the minimum value on the misfit map and are marked by the black star. Note the significant differences in the splitting parameters from the two events recorded by the same station due to different piercing point locations.

For XKS splitting, the seismograms were initially windowed in the time period 5 s before and 20 s after the predicted time of the XKS arrival, and were band-pass filtered in the frequency range of 0.04-0.5 Hz. The corresponding parameters for local S splitting are 5 s before and 10 s after, and 0.1-1.0 Hz. Then, we manually checked all the measurements to verify and (if necessary) adjust the beginning and end times of the XKS and local S window, quality ranking, and band-pass filtering frequencies. The final SWS measurements were grouped into Quality A (outstanding), B (good), N (null), and C (not used), and only A and B measurements were used in the study. Null measurements, which are characterized by robust XKS arrival on the original radial but no XKS energy

on the original transverse components, were not used in the study because all the stations with clear XKS arrivals on the radial components resulted in at least one Quality A or B measurement. Figure 2 exhibits example XKS measurements recorded at station RND from two events with different back azimuths, while Figure 3 shows local S wave splitting measurements from three different stations.

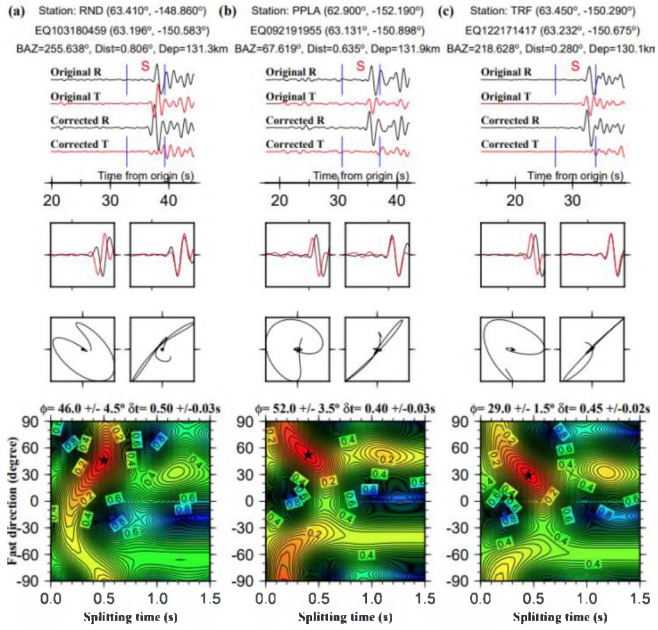

Figure 3. Examples of local S measurements from stations RND, PPLA, and TRF. Note that the corrected radial and corrected transverse components are relative to the pre-splitting shear wave polarization orientation rather than the back azimuth of the event.

4. RESULTS

A total of 971 pairs of well-defined (Quality A or B) XKS measurements (Figure 4a) were obtained at 106 stations, while 65 pairs of local S measurements (Figure 4b) were measured at 10 stations. For the XKS results, the fast orientations have a circular

mean value of 55.0° ± 37.4° and the splitting times range from 0.40 to 2.15 s with an average of 1.14 ± 0.31 s, which is slightly larger than the global average of 1.0 s for continents (Silver, 1996). For the local S splitting measurements, the averages are 62.4° ± 27.1° and 0.39 ± 0.13 s for the fast orientations and splitting times, respectively.

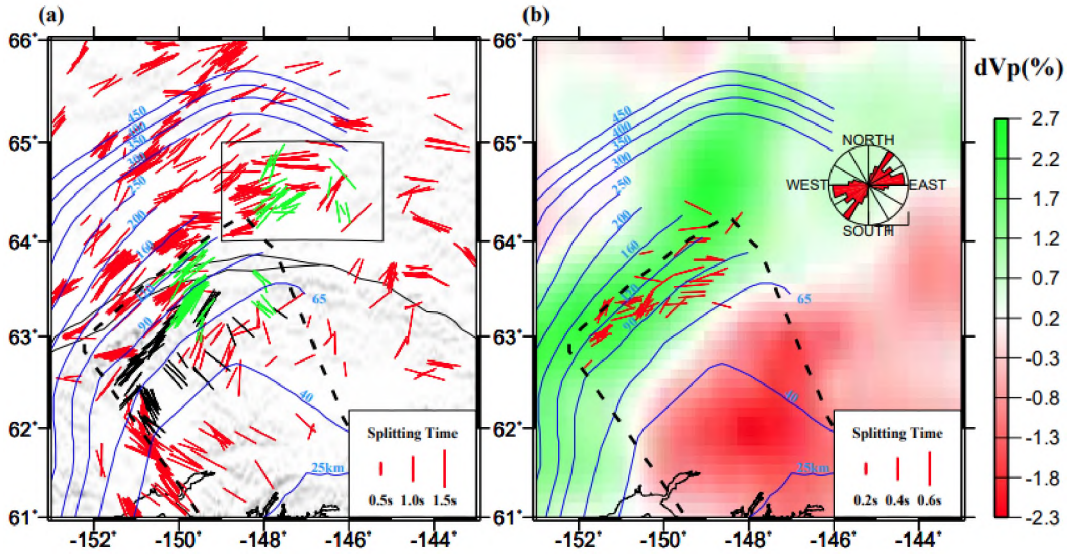

Figure 4. (a) 971 pairs of XKS splitting measurements from this study. Red bars stand for the splitting measurements from stations with azimuthally invariant measurements, black bars represent the splitting results showing systematic azimuthal variations with a 90° periodicity, and green bars indicate the splitting results exhibiting azimuthal variations without a 90° periodicity. All the measurements are plotted at the surface projections of the ray-piercing points at the depth of 200 km. Measurements in the black rectangle are used for anisotropy depth analysis shown in Figure 7. (b) 65 pairs of local shear wave splitting measurements and the rose diagram of the fast orientations. The background color shows the P wave velocity anomaly at 200 km depth (Gou et al., 2019).

4.1. CHARACTERIZATION OF COMPLEX ANISOTROPY

Two-layered anisotropy is considered as the most common form of complex anisotropy and the two pairs of splitting parameters can be determined using a grid-searching technique (Silver & Savage, 1994). Similar to previous complex anisotropy

studies (e.g., Cherie et al., 2016; Kong et al., 2018; Yang et al., 2014), measurements from 10 nearby stations with similar azimuthal variations (Figure 5) are combined in this study to improve the azimuthal coverage of the XKS events (black bars in Figure 4a). The resulting upper layer fast orientation is 47° which is nearly trench-parallel and has a splitting time of 0.7 s, while the fast orientation for the lower layer is 8° with a splitting time of 0.6 s (Figure 5).

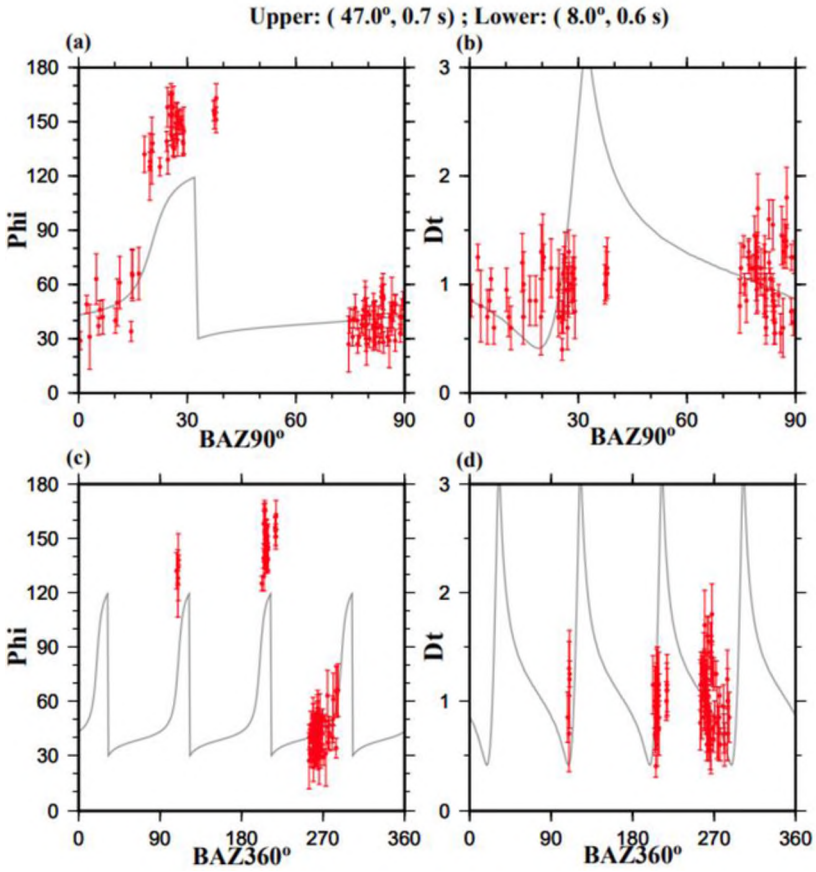

Figure 5. Systematic azimuthal variation of the combined XKS splitting measurements (black bars in Figure 4a). (a). Fast orientations plotted against modulo-90° back azimuth. (b). Splitting times against modulo-90° back azimuth. (c). Fast orientations against BAZ. (d). Splitting times against BAZ. The gray line in each plot represents the theoretical apparent splitting parameters calculated using the resultant optimal two pairs of parameters shown at the top of the figure.

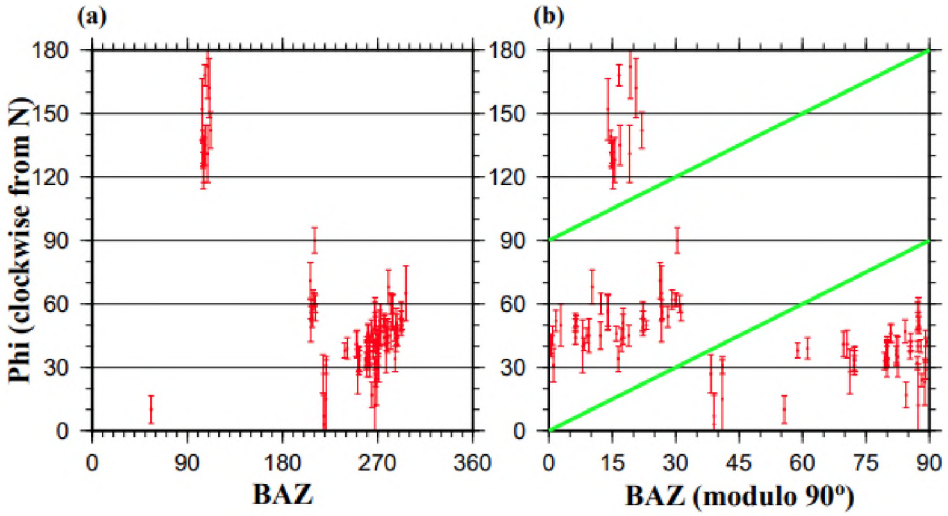

Figure 6. Azimuthal variation of the combined measurements (green bars in Figure 4a) showing spatially varying anisotropy. (a). Fast orientations against the back azimuth. (b). Fast orientations against modulo-90° back azimuth.

Measurements from several stations (green bars in the black rectangle in Figure 4a) also exhibit azimuthal variations but without a 90o or 180o periodicity (Figure 6), indicative of the possible existence of spatially varying (or piercing-point dependent) anisotropy. All the measurements from the northwest are trench-parallel, similar to the local S results, while those from the southeast are nearly NW-SE. Spatially varying anisotropy may reflect one anisotropy layer with different anisotropic characteristics (Alsina & Snieder, 1995; Liu & Gao, 2013), thereby implying a possible boundary that separates two or more areas with different anisotropy properties. We apply the spatial coherency approach to estimate the depth of the source of the observed anisotropy (Gao & Liu, 2012) using measurements from stations in the black rectangle in Figure 4a. The approach is based on the criterion that the optimal anisotropy depth corresponds to the highest spatial coherency reflected by the lowest spatial variation factor. The optimal anisotropy depth is searched in the range of 0 to 400 km with an interval of 5 km, and the

block size (dx) ranging from 0.22o to 0.30o are employed with a 0.02o interval. The anisotropy depth results are shown in Figure 7, in which all spatial variation factor curves indicate an estimated depth of ~250 km, comparable with the regional slab depth proposed by seismic tomography studies (e.g., Gou et al., 2019).

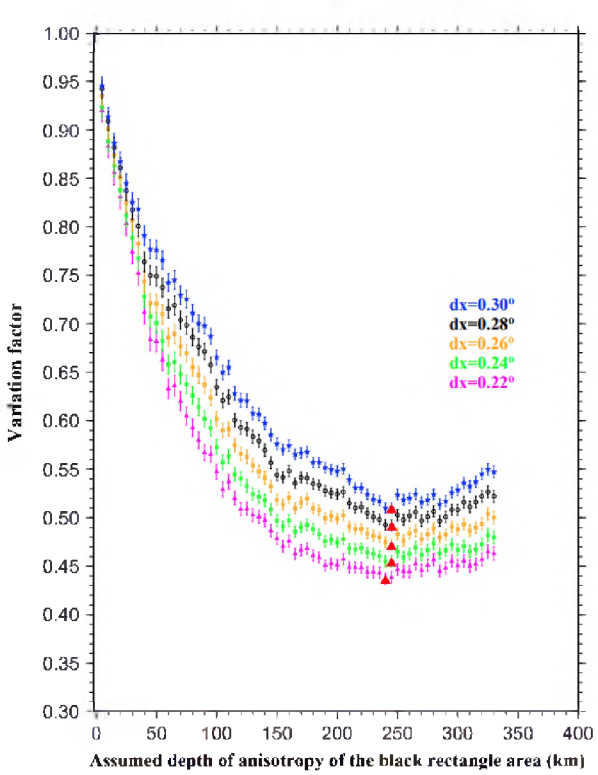

Figure 7. Spatial variation factors plotted against assumed depth of anisotropy for the XKS splitting measurements in the region outlined by the black rectangle in Figure 4a. Different curves are obtained using different dx values. The red triangles on the curves represent the minimum variation factors corresponding to the optimal depths of anisotropy.

4.2. SPATIAL DISTRIBUTION OF THE SPLITTING OBSERVATIONS

The study area is divided into 4 sub-regions (Figure 8) based on the characteristics of the XKS measurements. Area A includes the southmost portion of the

subducted YT and includes 138 measurements from 18 stations. The circular mean of the fast orientations is 140.7° ± 14.8° and the mean splitting time is 1.15 ± 0.31s, both are consistent with those obtained by previous studies (Christensen & Abers, 2010; Hanna & Long, 2012; McPherson et al., 2020; Venereau et al., 2019). Almost all the stations located south of the ~40 km slab depth contour line show trench-perpendicular fast orientations, which change to a nearly N-S direction where the slab descends more steeply.

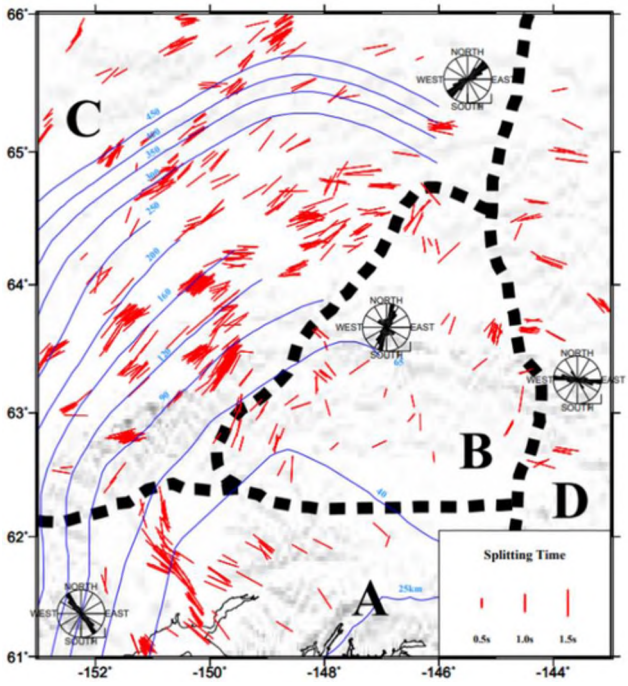

Figure 8. Subdivision of the study area based on the spatial distribution of XKS splitting measurements. All the measurements are plotted above the 200 km ray-piercing points. Black dash lines are the boundaries between the subregions (A-D). Each rose diagram indicates the fast orientations in each subregion.

Area B includes the NE portion of the YT and an area east of the Pacific-Yakutat slab edge, with 67 measurements from 14 stations. The mean value of the fast

orientations and the splitting times is 15.3° ± 37.5° and 0.90 ± 0.27 s, respectively. The standard deviation of the fast orientations is the largest, and the mean value of the splitting times is the lowest, among the four regions. The YT portion of this area is dominated by NE-SW fast orientations, while fast orientations in the eastern part of the area, which is located to the immediate east of the slab edge, are mostly in N-S directions.

Area C includes most part of the steeply dipping portion of the Pacific-Yakutat slab. The area contains 640 measurements from 47 stations. The circular mean of the fast orientations is 55.4° ± 20.5° and the simple mean of the splitting times is 1.17 ± 0.11 s, which is the highest in the study area. The fast orientations show a general parallelism with the strike of the slab depth contours, i.e., NE-SW in the western part of the area and gradually rotate to E-W and then WNW-ESE near the slab edge, similar to those obtained from previous SWS studies (McPherson et al., 2020; Venereau et al., 2019). This region contains all the 65 pairs of local S splitting measurements from 10 stations (Figure 4b), with mean values of 62.4° ± 27.1° and 0.39 ± 0.13 s for the fast orientations and splitting times, respectively. At the same 10 stations, the average XKS fast orientation is 53.2° ± 27.1°, which is similar to the average fast orientation of the local S results, and the mean splitting time is 1.25 ± 0.30 s, which is much larger than that of the local S results.

Area D is the easternmost part of the study area and includes 43 measurements from 5 stations. It is differentiated from Areas B and C by its dominantly WNW-ESE fast orientations (with a mean value of 100.1° ± 23.1°), similar to those in the northeastern part of Area C. The mean splitting time is 1.10 ± 0.32 s. These measurements are consistent with those from previous SWS studies.

5. DISCUSSION

The major features of the XKS and local S splitting measurements as well as results from two-layer fitting and depth estimate, can be accounted for by a model involving three flow systems, including an entrained flow beneath the flat subducting portion of the YT (Area A), a slab rollback driven toroidal flow system that includes a trench-parallel flow in the sub-slab region and a branch that goes around the slab edge and enters the mantle wedge, and an eastward continuation of the sub-slab flow after it passes the slab edge (Figures 9 and 10).

5.1. ENTRAINED FLOW BENEATH THE FLAT-SUBDUCTING YT

Both modeling and observational studies suggest that when the subducting lithosphere and the underlain asthenosphere are coupled, an entrained flow system reflecting the simple shear between the two layers can be generated, leading to trench-normal fast orientations (Jadamec & Billen, 2012; Russo & Silver, 1994). This type of mantle flow has been commonly observed in flat and shallow subduction zones, such as the Peruvian segment of the Peru-Chile subduction zone (Eakin & Long, 2013), the western Hellenic subduction zone (Olive et al., 2014), and the flat-subducting portion of the YT (Christensen & Abers, 2010; Hanna & Long, 2012; McPherson et al., 2020; Perttu et al., 2014; Venereau et al., 2019). The dominantly trench-normal fast orientations observed in Area A can thus be attributed to plastic flow entrained by the flat-subducting YT. Anisotropy in the lower layer obtained using stations in the junction zone of Areas

A, B, and C has a nearly N-S fast orientation (Figure 5), which is consistent with the dominant fast orientation in Area A and can also be attributed to entrained flow.

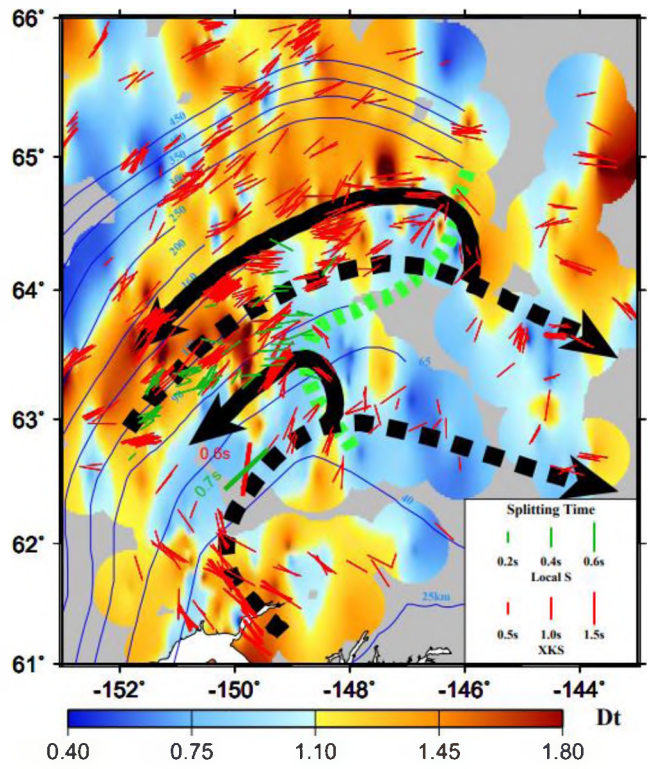

Figure 9. Schematic diagram showing direction of flow lines. The solid lines represent flow entering the mantle wedge from the sub-slab region, and the dashed lines mark the rollback-induced strike-parallel flow beneath the slab and its continued portion. Thin red and green bars are individual XKS and local S measurements, respectively. The thick red and green bars respectively indicate the lower and upper splitting parameters in the area with two-layered anisotropy. The thick dashed green line is the approximate slab edge, conjected from the spatially varying anisotropy. The background basemap shows spatially smoothed XKS splitting times.

5.2. SUB-SLAB TRENCH PARALLEL FLOW FROM SLAB ROLLBACK

Trench parallel fast orientations observed in the southern part of Area C can be attributed to sub-slab trench parallel flow induced by slab rollback (e.g., Fouch & Fischer, 1996; Hall et al., 2000; Jadamec & Billen, 2010, 2012; Russo & Silver, 1994)

with possible contributions from along-strike variations in slab dip (Kneller & Van Keken, 2008). Due to the high buoyancy of the YT, most studies suggest that slab rollback is insignificant in the study area. However, rollback of the "normal-dipping" section of the Pacific-Yakutat slab to the southwest of the YT has been suggested by some previous studies (e.g., Schellart et al., 2007), which should be capable of producing a sub-slab trench parallel flow that is responsible for the observed trench-parallel anisotropy in the southern part of Area C. Indeed, trench parallel fast orientations have been similarly observed along the entire Alaskan portion of the Aleutian subduction zone (McPherson et al., 2020; Venereau et al., 2019), indicating that variations in slab dip in the study area may not play a significant role in the observed trench parallel fast orientation.

5.3. CONTRIBUTION OF TRENCH-PARALLEL FLOW IN THE MANTLE WEDGE TO THE OBSERVED ANISOTROPY

The fast orientations observed in Areas A and C show a drastic variation from trench-perpendicular to trench-parallel. Based on the azimuthal and spatial variations of the SWS results, previous studies indicate that the ~70 km slab depth contour line represents the boundary separating the two fast orientation patterns, reflecting the sub-slab entrained flow and the trench-parallel flow in the wedge, respectively (Christensen & Abers, 2010; Hanna & Long, 2012; McPherson et al., 2020; Perttu et al., 2014; Venereau et al., 2019). However, the average splitting time from the local S measurements is only 0.39 ± 0.13 s, while the XKS results from the same 10 stations show a mean value of 1.25 ± 0.30 s, suggesting that contributions from trench parallel flow in the mantle wedge to the observed anisotropy is about half of that from the sub-

slab region. It should be mentioned that the splitting time of the upper layer from fitting of the apparent splitting parameters observed in the junction area of Areas A, B, and C is considerably larger (0.7 s) than that from local S wave SWS analysis, possibly due to the fact that the two areas do not exactly overlap, and to the different frequency compositions of the two types of waves.

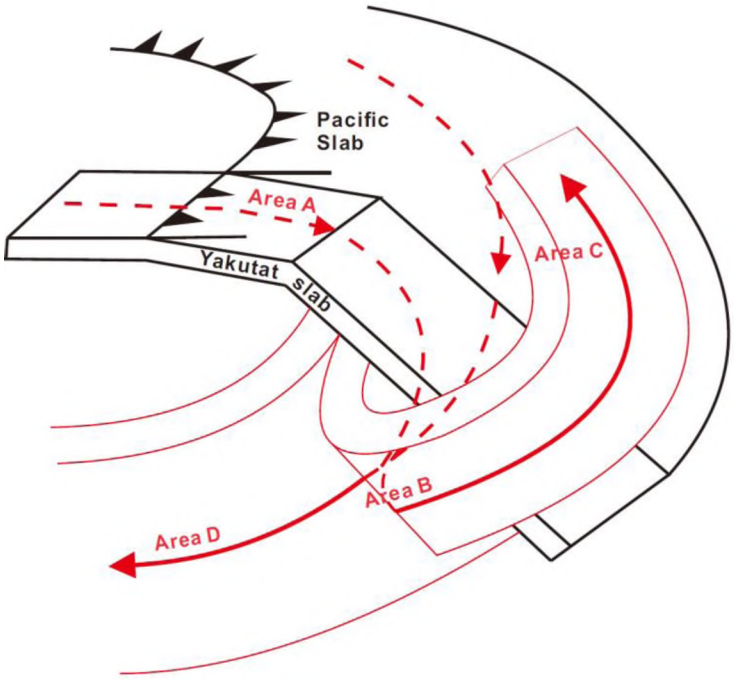

Figure 10. A three-dimensional schematic model showing the mantle flow fields in the four areas of the study area. Solid red arrows represent the flowlines outside of the slab, and dashed arrows indicate those beneath the slab. The two red columns represent the two flow branches. The sawteeth mark the trench of the Alaska subduction zone.

5.4. CONTINUATION OF SUB-SLAB MANTLE FLOW TOWARD THE EAST

The dominantly E-W and WNW-ESE measurements in Area D are in alignment with the local NW-striking strike-slip faults (e.g., Denali Fault in Figure 1a). McPherson

et al. (2020) suggest that the anisotropy here is caused by the shear deformation associated with the strike-slip boundary because of the directional similarity between the boundary trend and SWS fast orientations. The general validity of such an interpretation is essentially based on the hypothesis of vertical coherent deformation (Silver & Chan, 1991) advocating that the lithospheric mantle would deform consistently with the strike-slip processes in the crust and generate progressive simple shear. However, if lithospheric shear zones are the major contributors to the observed anisotropy in Area D, one would expect greater splitting times in areas of known shear zones (such as the Denali Fault). This spatial correspondence is not observed (Figure 9), and thus lithospheric fabrics may not be the major factor in generating the observed anisotropy in this area.

An alternative mechanism for the observed anisotropy in this region is an ESE-ward continuation of the sub-slab flow system, which splits into two branches after passing the slab edge: a toroidal branch entering the mantle wedge (see below), and a continuation branch. In the area immediately to the east of the slab edge (Area B), the moving directions of the two branches are approximately orthogonal to each other, leading to small splitting times (Silver & Savage, 1994).

5.5. TOROIDAL MANTLE FLOW AROUND THE SLAB EDGE

Geodynamic modeling investigations have demonstrated the presence of a toroidal component of mantle flow near a slab edge, where sub-slab trench parallel flow moves around the slab edge and enters the mantle wedge (Jadamec & Billen, 2010, 2012; Kincaid & Griffinths, 2003).

However, the predicted flow direction in the mantle wedge beneath most part of Area C is trench normal, which is different from the observed fast orientations of local S waves (which mostly sample the mantle wedge) in this area by ~90o. In addition to the possible reasons for this discrepancy discussed by McPherson et al. (2020), we speculate that the proposed westward increase in the trench retreat rate (from 0.6 cm/yr in south central Alaska to 1.9 cm/yr in the central Aleutians) by Schellart et al. (2007) may cause the transported materials from the sub-slab region to flow further away from the slab edge along the slab. The observed large splitting times and trench parallel fast orientations (Figure 9) can thus be attributed to the combined effects of two anisotropic layers with similar fast orientations associated with trench-parallel flows in both the mantle wedge and the sub-slab region.

6. CONCLUSIONS

SWS measurements from both teleseismic and local events are utilized to constrain mantle flow patterns beneath south central Alaska. The vast majority of the observations, together with results from complex anisotropy analysis and depth estimation of the source of the observed anisotropy, can be explained by a model invoking the splitting of the sub-slab trench-parallel flow into two branches. One of the branches is a continuation of the sub-slab flow system toward the ESE direction, and the other branch flows around the slab edge, enters the mantle wedge, and flows toward the SW along the slab. The two branches are approximately orthogonal to each other in the

area immediately to the east of the slab edge, producing spatially varying fast orientations with smaller than normal splitting times.

REFERENCES

Alsina, D., & Snieder, R. (1995). Small-scale sublithospheric continental mantle deformation: Constraints from SKS splitting observations. Geophysical Journal International, 123, 431-448.

Ando, M., 1984. ScS polarization anisotropy around the Pacific Ocean. Journal of Physics of the Earth, 32, 179-196.

Cherie, S. G., Gao, S. S., Liu, K. H., Elsheikh, A. A., Kong, F., Reed, C. A., & Yang, B. B. (2016). Shear wave splitting analyses in Tian Shan: Geodynamic implications of complex seismic anisotropy. Geochemistry, Geophysics, Geosystems, 17, 1975-1989. doi:10.1002/2016GC006269

Christensen, D. H., & Abers, G. A. (2010). Seismic anisotropy under central Alaska from SKS splitting observations. Journal of Geophysical Research, 115, B04315. doi:10.1029/2009JB006712

Civello, S., & Margheriti, L. (2004). Toroidal mantle flow around the Calabrian slab (Italy) from SKS splitting. Geophysical Research Letters, 31(10), L10601, 2001-2004. https://doi.org/10.1029/2004GL019607

Currie, C. A., Cassidy, J. F., Hyndman, R. D., & Bostock, M. G. (2004). Shear wave anisotropy beneath the Cascadia subduction zone and western North America craton. Geophysical Journal International, 157, 341-353. doi:10.1111/j.1365-246X.2004.02175.x

Dahm, H. H., Gao, S. S., Kong, F. & Liu, K. H. (2017). Topography of the mantle transition zone discontinuities beneath Alaska and its geodynamic implications: Constraints from receiver function stacking. Journal of Geophysical Research: Solid Earth, 122, 10,352-10,363. https://doi.org/10.1002/2017JB014604

Eakin, C. M., & Long, M. D. (2013). Complex anisotropy beneath the Peruvian flat slab from frequency-dependent, multiple-phase shear wave splitting analysis. Journal of Geophysical Research: Solid Earth, 118, 4794-4813. doi:10.1002/jgrb.50349

Eberhart-Phillips, D., Christensen, D. H., Brocher, T. M., Hansen, R., Ruppert, N. A., Haeussler, P. J., & Abers, G. A. (2006). Imaging the transition from Aleutian subduction to Yakutat collision in central Alaska, with local earthquakes and active source data. Journal of Geophysical Research, 111, B11303. Doi:10.1029/2005JB004240

Feng, L., Liu, C., & Ritzwoller, M. H. (2020). Azimuthal anisotropy of the crust and uppermost mantle beneath Alaska. Journal of Geophysical Research: Solid Earth, 125, e2020JB020076, https://doi.org/10.1029/2020JB020076

Ferris, A., Abers, G. A., Christensen, D. H., & Veenstra, E. (2003). High resolution image of the subducted Pacific (?) plate beneath central Alaska, 50-150 km depth. Earth and Planetary Science Letters, 214(3–4), 575–588. https://doi.org/10.1016/S0012-821X(03)00403-5

Fouch, M. J., & Fischer, K. M. (1996). Mantle anisotropy beneath northwest Pacific subduction zones. Journal of Geophysical Research: Solid Earth, 101(B7), 15,987-16,002. https://doi.org/10.1029/96jb00881

Gao, S. S., & Liu, K. H. (2012). AnisDep: A FORTRAN program for the estimation of the depth of anisotropy using spatial coherency of shear-wave splitting parameters. Computers & Geosciences, 49, 330-333. doi:10.1016/j.cageo.2012.01.020

Gou, T., Zhao, D., Huang, Z., & Wang, L. (2019). Aseismic deep slab and mantle flow beneath Alaska: Insight from anisotropic tomography. Journal of Geophysical Research: Solid Earth, 124, 1700-1724. https://doi.org/10.1029/2018JB016639

Hanna, J., & Long, M. D. (2012). SKS splitting beneath Alaska: Regional variability and implications for subduction processes at a slab edge. Tectonophysics, 530-531, 272-285. https://doi.org/10.1016/j.tecto.2012.01.003

Hess, H. H. (1964), Seismic anisotropy of the uppermost mantle under oceans. Nature, 203, 629-631.

Jadamec, M. A., & Billen, M. I. (2010). Reconciling surface plate motions with rapid three-dimensional mantle flow around a slab edge. Nature, 465, 338-341. https://doi.org/10.1038/nature09053

Jadamec, M. A., & Billen, M. I. (2012). The role of rheology and slab shape on rapid mantle flow: Three-dimensional numerical models of the Alaska slab edge. Journal of Geophysical Research: Solid Earth, 117, B02304. https://doi.org/10.1029/2011JB008563

Jiang, C., Schmandt, B., Ward, K. M., Lin, F. C., & Worthington, L. L. (2018). Upper mantle seismic structure of Alaska from Rayleigh and S wave tomography. Geophysical Research Letters, 45, 10,350-10,359. https://doi.org/10.1029/2018GL079406

Jiang, E., Liu, K. H., Gao, Y., Fu, X., & Gao, S. S. (2021). Spatial variations of upper crustal anisotropy along the San Jacinto Fault Zone in Southern California: Constraints from shear wave splitting analysis. Journal of Geophysical Research: Solid Earth, 126, e2020JB020876. https://doi.org/10.1029/2020JB020876

Karlowska, E., Bastow, I. D., Rondenay, S., Martin-Short, R., & Allen, R. M. (2021). The development of seismic anisotropy below south-central Alaska: Evidence from local earthquake shear wave splitting. Geophysical Journal International, 225(1), 548-554. https://doi.org/10.1093/gji/ggaa603

Kincaid, C., & Griffiths, R. W. (2003). Laboratory models of the thermal evolution of the mantle during rollback subduction. Nature, 425(6953), 58-62. https://doi.org/10.1038/nature01923

Kneller, E. A., & van Keken, P. E. (2008). Effect of three-dimensional slab geometry on deformation in the mantle wedge: Implications for shear wave anisotropy. Geochemistry, Geophysics, Geosystems, 9, Q01003. https://doi.org/10.1029/2007GC001677

Kong, F., Wu, J., Liu, L., Liu, K. H., Song, J., Li, J., & Gao, S. S. (2018). Azimuthal anisotropy and mantle flow underneath the southeastern Tibetan Plateau and northern Indochina Peninsula revealed by shear wave splitting analyses. Tectonophysics, 747-748, 68–78. https://doi.org/10.1016/j.tecto.2018.09.013

Kong, F., Gao, S. S., Liu, K. H., Ding, W. W., & Li, J. (2020). Slab dehydration and mantle upwelling in the vicinity of the Sumatra subduction zone: Evidence from receiver function imaging of mantle transition zone discontinuities. Journal of Geophysical Research: Solid Earth, 125, e2020JB019381. https://doi.org/10.1029/2020JB019381

Liu, K. H., & Gao, S. S. (2011). Estimation of the depth of anisotropy using spatial coherency of shear-wave splitting parameters. Bulletin of the Seismological Society of America, 101, 2153-2161. https://doi.org/10.1785/0120100258

Liu, K. H., & Gao, S. S. (2013). Making reliable shear-wave splitting measurements. Bulletin of the Seismological Society of America, 103(5), 2680–2693. https://doi.org/10.1785/0120120355

Long, M. D., & Becker, T. W. (2010). Mantle dynamics and seismic anisotropy. Earth and Planetary Science Letters, 297(3-4), 341–354. https://doi.org/10.1016/j.epsl.2010.06.036

Long, M. D., & Silver, P. G. (2008). The subduction zone flow field from seismic anisotropy: A global view. Science, 319(5861), 315-318. https://doi.org/10.1126/science.1150809

Long, M. D., & Silver, P. G. (2009). Shear wave splitting and mantle anisotropy: Measurements, interpretations, and new directions. Surveys in Geophysics, 30(4–5), 407–461. https://doi.org/10.1007/s10712-009-9075-1

Martin-Short, R., Allen, R., Bastow, I. D., Porritt, R. W., & Miller, M. S. (2018). Seismic imaging of the Alaska subduction zone: Implications for slab geometry and volcanism. Geochemistry, Geophysics, Geosystems, 19(11), 4541-4560. https://doi.org/10.1029/2018GC007962

McPherson, A. M., Christensen, D. H., Abers, G. A., & Tape, C. (2020). Shear wave splitting and mantle flow beneath Alaska. Journal of Geophysical Research: Solid Earth: Solid Earth, 123, e2019JB018329, https://doi.org/10.1029/2019jb018329

Olive, J. A., Pearce, F., Rondenay, S., & Behn, M. D. (2014). Pronounced zonation of seismic anisotropy in the Western Hellenic subduction zone and its geodynamic significance. Earth and Planetary Science Letters, 391, 100-109. https://doi.org/10.1016/j.epsl.2014.01.029

Paczkowski, K., Montési., L. G. J., Long, M. D., & Thissen, C. J. (2014). Three-dimensional flow in the subslab mantle. Geochemistry, Geophysics, Geosystems, 15, 3989-4008. https://doi.org/10.1002/ 2014GC005441

Palano, M., Piromallo, C., & Chiarabba, C. (2017). Surface imprint of toroidal flow at retreating slab edges: The first geodetic evidence in the Calabrian subduction system. Geophysical Research Letters, 44(2), 845-853. https://doi.org/10.1002/2016GL071452

Perttu, A., Christensen, D., Abers, G., & Song, X. (2014). Insights into mantle structure and flow beneath Alaska based on a decade of observations of shear wave splitting. Journal of Geophysical Research: Solid Earth, 119, 8366-8377. https://doi.org/10.1002/2014JB011359

Ribe, N. M., & Yu , Y. (1991). A theory for plastic deformation and textural evolution of olivine polycrystals. Journal of Geophysical Research: Solid Earth, 96, 8325-8335.

Russo, R. M., & Silver, P. G. (1994). Trench-parallel flow beneath the Nazca plate from seismic anisotropy. Science, 263(5150), 1105-1111. https://doi.org/10.1126/science.263.5150.1105

Schellart, W. P. (2004). Kinematics of subduction and subduction-induced flow in the upper mantle. Journal of Geophysical Research: Solid Earth, 109(7), B07401. https://doi.org/10.1029/2004JB002970

Schellart, W. P., Freeman, J., Stegman, D. R., Moresi, L., & May, D. (2007). Evolution and diversity of subduction zones controlled by slab width. Nature, 446(7133), 308–311. https://doi.org/10.1038/nature05615

Silver, P. G. (1996). Seismic anisotropy beneath the continents: Probing the depths of geology. Annual Review of Earth and Planetary Sciences, 24, 385-432. https://doi.org/10.1146/annurev.earth.24.1.385

Silver, P. G., & Chan, W. W. (1991). Shear wave splitting and subcontinental mantle deformation. Journal of Geophysical Research, 96, B10, 16,429-16,454.

Silver, P. G., & Savage, M. K. (1994). The interpretation of shear-wave splitting parameters in the presence of two anisotropic layers. Geophysical Journal International, 119, 949–963.

Tian, Y., & Zhao, D. (2012). Seismic anisotropy and heterogeneity in the Alaska subduction zone. Geophysical Journal International, 190(1), 629-649. https://doi.org/10.1111/j.1365-246X.2012.05512.x

Venereau, C. M. A., Martin-Short, R., Bastow, I. D., Allen, R. M., & Kounoudis, R. (2019). The role of variable slab dip in driving mantle flow at the eastern edge of the Alaskan subduction margin: Insights from shear-wave splitting. Geochemistry, Geophysics, Geosystems, 20, 2433–2448. https://doi.org/10.1029/2018GC008170

Vinnik, L. P., Makeyeva, L. I., Milev, A., & Usenko, A. Y. (1992). Global patterns of azimuthal anisotropy and deformations in the continental mantle. Geophysical Journal International, 111(3), 433-447. https://doi.org/10.1111/j.1365-246X.1992.tb02102.x

Worthington, L. L., Van Avendonk, H. J. A., Gulick, S. P. S., Christeson, G. L., & Pavlis, T. L. (2012). Crustal structure of the Yakutat terrane and the evolution of subduction and collision in southern Alaska. Journal of Geophysical Research: Solid Earth, 117(1), 1-20. https://doi.org/10.1029/2011JB008493

Yang, B. B., Gao, S. S., Liu, K. H., Elsheikh, A. A., Lemnifi, A. A., Refayee, H. A., & Yu, Y. (2014). Seismic anisotropy and mantle flow beneath the northern Great Plains of North America. Journal of Geophysical Research: Solid Earth, 119, 1971–1985. https://doi.org/10.1002/2013JB010561

Zhang, S., & Karato, S. (1995). Lattice preferred orientation of olivine aggregates deformed in simple shear. Nature, 375, 774-777. https://doi.org/10.1038/375774a0

SECTION

2. CONCLUSIONS

In this research, we use all available broadband seismic data obtained from USArray Transportable Array (TA) and other seismic stations to investigate the upper mantle flow and the corresponding anisotropy structures in the contiguous Alaska region. Finally, a total of 2790 pairs of well-defined splitting measurements are obtained, and some significant findings are reportable, as listed below:

1). Multiple mantle flow fields are detected beneath the entire Alaska region. In southern Alaska where the subduction process is ongoing, the regional mantle flow system is strongly controlled by slab geometry and subducting approach. The mantle flow is dominantly trench-parallel beneath the normal-dipping Pacific slab, while the flow beneath the flat Yakutat slab is initially trench-perpendicular and subsequently deflects to a trench-parallel direction as the slab descends more steeply. A toroidal flow pattern is observed near the Pacific-Yakutat slab edge. Such flow transfers sub-slab mantle materials to the mantle wedge through a three-dimensional circulation. By contrast, the mantle flow in the tectonically stable northern Alaska is dominantly APM-parallel, with possible deflections induced by the deep continental keel.

2). Complex anisotropy is characterized in three regions in the vicinity of the Alaska subduction zone. The anisotropy structure in region ENT indicates the confluence of different flow systems at different depths. Region SEA shows a two-layered structure that consists of a lower asthenospheric flow possibly escaped from the Yakutat slab

window or induced by the APM, under the assumption of an upper compression-induced lithospheric anisotropy layer. Region CEN also exhibits two anisotropic layers, corresponding to the trench-parallel flow in the mantle wedge and sub-slab entrained flow, respectively. In addition, the examination of spatially varying anisotropy indicates the possible location of the Pacific-Yakutat slab edge.

3). The slab rollback-induced sub-slab flow may separate into two branches at the edge: One branch flows in an anticlockwise direction, generating substantial trench-parallel flow in the mantle wedge. The other continues flowing to the eastern Alaksa.

BIBLIOGRAPHY

Christensen, D. H., & Abers, G. A. (2010). Seismic anisotropy under central Alaska from SKS splitting observations. Journal of Geophysical Research, 115(B4), 1–12. https://doi.org/10.1029/2009jb006712

Hanna, J., & Long, M. D. (2012). SKS splitting beneath Alaska: Regional variability and implications for subduction processes at a slab edge. Tectonophysics, 530–531, 272–285. https://doi.org/10.1016/j.tecto.2012.01.003

Long, M. D., & Silver, P. G. (2009). Shear wave splitting and mantle anisotropy: Measurements, interpretations, and new directions. Surveys in Geophysics, 30(4–5), 407–461. https://doi.org/10.1007/s10712-009-9075-1

McPherson, A. M., Christensen, D. H., Abers, G. A., & Tape, C. (2020). Shear wave splitting and mantle flow beneath alaska. Journal of Geophysical Research: Solid Earth, 125(4), 1–18. https://doi.org/10.1029/2019jb018329

Perttu, A., Christensen, D., Abers, G., & Song, X. (2014). Insights into mantle structure and flow beneath Alaska based on a decade of observations of shear wave splitting. Journal of Geophysical Research, Solid Earth, 119, 8366–8377. https://doi.org/10.1002/ 2014JB011359.

Savage, M. S. (1999). Seismic anisotropy and mantle deformation: What have we learned from shear wave splitting? Reviews of Geophysics, 37(1), 65–106. https://doi.org/10.1029/98RG02075

Silver, P. G., & Chan, W. W. (1991). Shear wave splitting and subcontinental mantle deformation. Journal of Geophysical Research, 96, 16429–16454. https://doi.org/10.1017/S0002020600023313

Venereau, C. M. A., Martin-Short, R., Bastow, I. D., Allen, R. M., & Kounoudis, R. (2019). The role of variable slab dip in driving mantle flow at the eastern edge of the Alaskan subduction margin: Insights from shear-wave splitting. Geochemistry, Geophysics, Geosystems, 20(5), 2433–2448. https://doi.org/10.1029/2018GC008170

VITA

Yuchen Yang was born in Daqing city, China. He studied Resource Exploration Engineering at Northeast Petroleum University for the first two college years. Then he was transferred to Missouri University of Science and Technology for the remaining two years and studied Geology and Geophysics. Yuchen earned his two bachelor's degrees in May 2017 and joined the Geology and Geophysics program at Missouri University of Science and Technology to pursue his PhD degree in August, 2017.

Yuchen studied hard during his undergraduate years and gained the 4.0 GPA medal. During the graduate years, Yuchen's research focused on investigating the mantle structures and dynamics of the Alaska region. He presented his research works at the annual meeting of American Geophysical Union (AGU) in 2018 and 2019. He was an active member in Society of Exploration Geophysicists (SEG) and was elected as the president of SEG at Missouri University of Science and Technology chapter during the year 2019. He was also selected as one of the fifty worldwide SEG chapter leaders and subsequently joined the Student Leadership Symposium in San Antonio in 2019.

In July 2021 he received his PhD degree in Geology and Geophysics from Missouri University of Science and Technology.